The Kinematic Structure of a Wasatch Mountain Winter Storm during IPEX IOP3

JUSTIN A. W. COX,* W. JAMES STEENBURGH,* DAVID E. KINGSMILL,+ JASON C. SHAFER,*
BRIAN A. COLLE,# OLIVIER BOUSQUET,@ BRADLEY F. SMULL,& AND HUAQING CAI+

* *NOAA/Cooperative Institute for Regional Prediction, and Department of Meteorology, University of Utah, Salt Lake City, Utah*
\+ *Desert Research Institute, Reno, Nevada*
\# *Institute for Terrestrial and Planetary Atmospheres, State University of New York at Stony Brook, Stony Brook, New York*
@ *Department of Atmospheric and Oceanic Sciences, McGill University, Montreal, Quebec, Canada*
& *Department of Atmospheric Sciences, University of Washington, Seattle, Washington*

(Manuscript received 15 December 2003, in final form 2 August 2004)

ABSTRACT

The influence of orographic circulations on the precipitation structure of a Wasatch Mountain winter storm is examined using observations collected during the third intensive observing period (IOP3) of the Intermountain Precipitation Experiment (IPEX). The event featured the passage of a midlevel (700–550 hPa) trough followed 3 h later by a surface trough. Prior to and during the midlevel trough passage, large-scale southwesterly flow impinged on the Wasatch Mountains. Low-level confluence was observed between this southwesterly flow and along-barrier southerly flow within 20–40 km of the Wasatch Mountains. This confluence zone, which moved toward the Wasatch Mountains during and following the passage of the midlevel trough, was accompanied by low-level convergence and precipitation enhancement over the upstream lowlands. Dual-Doppler analysis revealed the presence of a shallow along-barrier jet near the base of the Wasatch Mountains that was surmounted by southwesterly cross-barrier flow at mid- and upper-mountain levels. This cross-barrier flow produced strong (1–2 m s^{-1}) ascent as it interacted with the steep windward slopes of the Wasatch Mountains, where precipitation was roughly double that observed in the lowlands upstream. Flow deflection and splitting were also observed near the highest terrain features. A narrow region of strong subsidence, which at times exceeded 2 m s^{-1}, was found to the lee of the Wasatch and, based on radar imagery, appeared to modulate hydrometeor spillover aloft. Processes contributing to the evolution of the near-barrier flow field, including topographic blocking, diabatic effects, and surface friction contrasts, are discussed.

1. Introduction

The narrow and intense vertical relief of the Wasatch Mountains in northern Utah contributes to the development of orographic snowstorms that impact cross-mountain commerce, mountain communities, and the densely populated Wasatch Front urban corridor. A primary goal of the U.S. Weather Research Program is to improve quantitative precipitation forecasting, with orographic precipitation identified as a research area poised for rapid progress (Smith et al. 1997; Fritsch et al. 1998). Precipitation is strongly modulated by orographic processes in the Intermountain West, which lies east of the Sierra Nevada and Cascade Mountains and west of the Continental Divide. Much of the Intermountain West is characterized by basin-and-range topography, which features narrow, steeply sloped mountain ranges separated by broad alluvial basins. The western slopes of the Wasatch Mountains of northern Utah rise 1200–2000 m in 5 km to elevations of more than 3350 m above mean sea level (MSL; Fig. 1), and near Ogden, Utah (OGD), are only ~10 km in width. The Wasatch Front urban corridor includes the cities of OGD, Salt Lake (SLC), and Provo (PVU; see Fig. 1a for locations). Winter storms in these cities produced $100 million in property damage over the four winter seasons from 1993/94 to 1996/97, and such socioeconomic impacts are increasing because of rapid population growth that approaches 30% decadally (Blazek 2000; Schultz et al. 2002). In mountain communities such as Alta (ATB), mean annual snowfall approaches 1300 cm, and storm-cycle accumulations can reach 250 cm (e.g., Steenburgh 2004).

A large body of literature has examined orographic precipitation processes over ranges such as the Tushar Mountains and the Wasatch Plateau of central Utah (e.g., Sassen et al. 1986; Long et al. 1990; Sassen et al. 1990; Huggins 1995), the Park Range of northern Colorado (e.g., Sassen 1984; Rauber et al. 1986; Rauber

---

Corresponding author address: Justin A. W. Cox, Dept. of Meteorology, University of Utah, 135 South 1460 East, Room 819, Salt Lake City, UT 84112.
E-mail: jacox@met.utah.edu

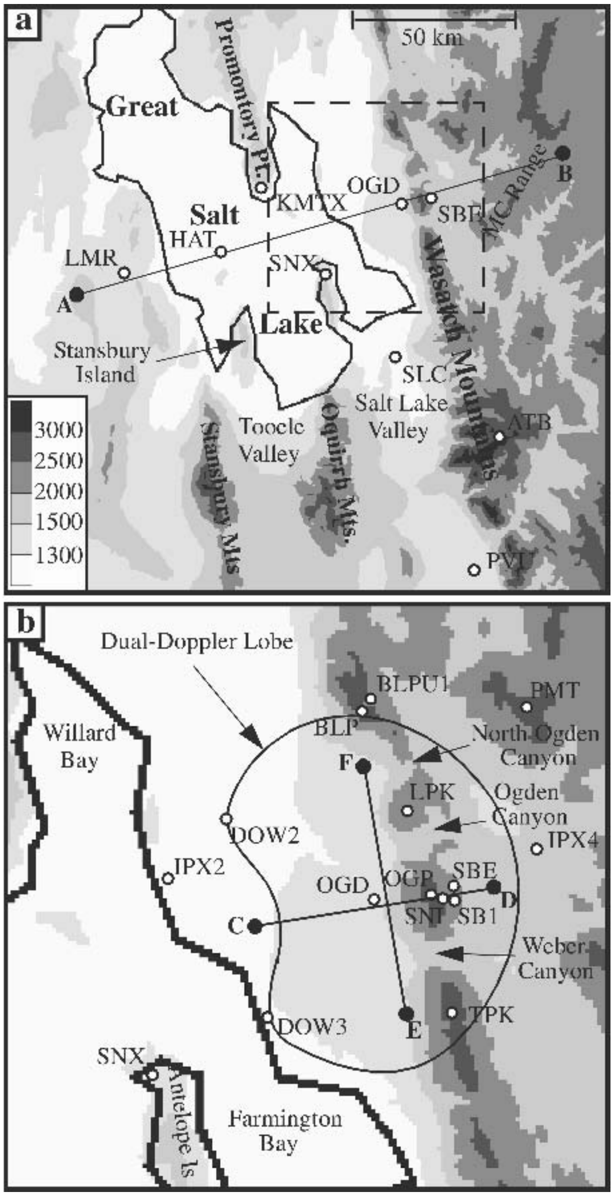

FIG. 1. Topographic and geographic features of (a) northern Utah and (b) the Wasatch Front near Ogden. Location abbreviations and station identifiers are Alta (ATB), Antelope Island (SNX), Ben Lomond Peak (BLP), Ben Lomond SNOTEL site (BLPU1), DOW2 site, DOW3 site, Hat Island (HAT), Huntsville (IPX4), Lewis Peak (LPK), Monte Cristo Range (MC Range), Oasis (LMR), Ogden (OGD), Ogden Peak (OGP), Powder Mountain (PMT), the Promontory Point WSR–88D (KMTX), Provo (PVU), Salt Lake City (SLC), Snowbasin–Base (SBE), Snowbasin–Middle Bowl (SNI), Snowbasin–Strawberry Base (SB1), Southern Causeway (IPX2), Syracuse (QSY), and Thurston Peak (TPK). Cross-section locations annotated. Terrain shading based on scale in lower left of (a).

and Grant 1986), the San Juan Mountains of southwest Colorado (e.g., Cooper and Saunders 1980; Marwitz 1980), the Cascade Mountains of Washington (e.g., Hobbs 1975), the Mogollon Rim of Arizona (e.g., Bruintjes et al. 1994; Klimowski et al. 1998; Reinking et al. 2000), and the Sierra Nevada of California (e.g., Marwitz 1987a,b; Heggli and Rauber 1988; Rauber 1992). However, only recently has dual-Doppler analysis been used to describe the kinematic structure of orographic storms. For example, Colle and Mass (1996) used the X-band (3.22 cm) tail-mounted radar on the National Oceanic and Atmospheric Administration (NOAA) WP-3D research aircraft to document flow splitting and precipitation enhancement on the southern slopes of the Olympic Mountains of Washington and downslope flow and rainshadowing to the lee. Using NOAA WP-3D and University of Oklahoma Doppler on Wheels (DOW) radar data collected during the Mesoscale Alpine Programme (MAP; Bougeault et al. 2001), Steiner et al. (2003) showed the development of downvalley flow within a deep Alpine valley that was surmounted by oppositely directed, orographically lifted flow aloft. The downvalley flow appeared to be produced by the evaporation and melting of orographic precipitation at low levels. Bousquet and Smull (2003a) further described the multiscale blocking effects during MAP using airborne radar observations, including flow channeling along the curved south face of the Alps and convective instability release windward of the Apennine Mountains. Such airborne Doppler radar data have also been used to show that upvalley flow may occur in deep Alpine valleys during unblocked orographic precipitation events (e.g., Bousquet and Smull 2003b).

This paper describes the kinematic structure of a winter storm over the Wasatch Mountains using data collected during the Intermountain Precipitation Experiment (IPEX). IPEX was held over northern Utah during February 2000 to improve the understanding and prediction of winter storms over the Intermountain West (Schultz et al. 2002). Detailed observations were collected during the third intensive observing period (IOP3) when up to 80 cm of snow fell in the Wasatch Mountains, producing the largest orographic precipitation event of the field program. IOP3 also featured intense spatial gradients in precipitation over the windward and leeward slopes of the Wasatch and precipitation enhancement over the upstream lowlands near OGD (Cox 2002; Shafer 2002). In the following analysis, emphasis is placed on determining the influence of orographic circulations upon the precipitation distribution of the event.

We begin by describing the datasets and methods used to perform the analysis, including dual-Doppler analysis techniques. In section 3, data from a number of observing platforms, including the NOAA WP-3D and two DOW radars, are used to describe the kinematic and precipitation structure of the event near the Wasatch Mountains. Section 4 presents a summary schematic and compares findings with other observational, numerical, and theoretical studies of orographic precipitation and airflow dynamics. The paper concludes with a summary and recommendations for future work.

2. Data and methods

During IOP3, the NOAA WP-3D research aircraft executed four multilevel flight stacks normal to the Wasatch Mountains and roughly parallel to the crest-level flow. Each stack featured two flight legs at and above crest level (oriented roughly along line A–B in Fig. 1a) and two flight legs at lower levels upstream of the Wasatch Mountains. Flight leg elevations were not fixed from stack to stack, but were occasionally modified to meet microphysical sampling needs. On some flight stacks, spiral ascents/descents were interlaced between flight legs. Airborne meteorological observations included 1-s flight-level observations of temperature, moisture, wind, and vertical velocity, as well as radar reflectivity from the tail-mounted X-band Doppler radar. An equipment problem limited the use of aft radar scans, thus preventing pseudo-dual-Doppler synthesis of the three-dimensional wind field along the flight track (e.g., Jorgensen et al. 1996). As a result, only tail-radar reflectivities are presented. At the surface, high-density observations were provided by National Severe Storms Laboratory (NSSL) mobile labs and by the MesoWest cooperative networks, which are managed by the University of Utah (Horel et al. 2002). Schultz et al. (2002) describe these datasets in detail.

For cross-section analyses, flight-level observations were time–space adjusted (Fujita 1963) to two observation times (1735 and 2035 UTC) corresponding to the launch of GPS radiosondes by NSSL mobile labs at Oasis (LMR) and OGD (see Fig. 1a for locations). Following Neiman and Shapiro (1993), this was done by assuming that the primary synoptic feature of the event, a midlevel trough, was in steady state and moving at a fixed-phase velocity. Errors can arise from these assumptions (see Neiman and Shapiro 1993), and a primary concern in the present case is that observations of the midlevel trough need to be time–space adjusted, whereas those of the orographic storm do not. To partially mitigate this concern, a time–space adjustment was used primarily to examine the structure of the storm windward of the Wasatch Mountains where the orographic response would likely be strongest at and below crest level. Since NSSL mobile laboratory soundings and MesoWest observations provided the majority of observations below crest level, the aircraft data were adjusted to the sounding launch times, which preserved the low-level kinematic and thermodynamic structure relative to the barrier. The WP-3D equivalent potential temperature with respect to ice (θ_{ei}) observations were also adjusted to account for a small ($\sim$1 K) bias relative to the NSSL radiosondes.

The near-barrier flow field was examined using data collected by two University of Oklahoma DOW X-band radars (Wurman et al. 1997), which were positioned beneath the flight stacks and just upstream of the Wasatch Mountains (Fig. 1b). The two DOWs (DOW2 and DOW3) were sited $\sim$20 km from the Wasatch crest and along a 20-km north–south baseline. The resulting dual-Doppler lobe covered the area between the mountain crest and the Great Salt Lake.

Radar volumes from each of the DOWs were analyzed at 20–30 min intervals from 1832 to 2134 UTC 12 February. DOW3 used a 180° plan position indicator (PPI) strategy with elevation angles of 1.0°, 2.4°, 3.4°, 4.5°, 5.5°, 6.5°, 7.9°, 9.9°, 11.9°, and 14.9°, scanning toward the Wasatch Mountains for all but one volume. DOW2 used a 360° PPI strategy with elevation angles of 0.0°, 1.3°, 2.5°, 3.5°, 4.5°, 5.5°, 6.5°, 7.9°, 9.9°, 11.9°, 14.9°, and 17.9° from 1832 to 2030 UTC. After 2030 UTC, DOW2 used the same scan strategy as DOW3.

DOW data were processed using software developed by the National Center for Atmospheric Research (NCAR). SOLO was used to reorient and edit the data, REORDER was used for the interpolation, and CEDRIC (Custom Editing and Display of Reduced Information in Cartesian Space) was used to perform the dual-Doppler synthesis and vertical integration (Mohr and Miller 1983). Reorientation was based on GPS locations of nearby ground clutter targets, such as powerline intersections and hedgerows. The data were then thresholded at a normalized coherent power (NCP) value of 0.4, and ground clutter was removed based on reflectivity and velocity signatures. No problems were encountered with velocity folding, or with sidelobe and second trip echoes. Beam blockage limited data coverage east of the high mountain peaks.

A Cressman (1959) distance-weighted scheme was used to interpolate the DOW data to a Cartesian grid with 500-m horizontal and vertical grid spacing. The radii of influence varied with height to improve data coverage while eliminating interpolation artifacts. From the lowest level (300 m above lake level) above radar elevation (1265 m MSL) to 3000 m MSL, the horizontal and vertical radii of influence were 500 m. Above 3000 m MSL, the vertical (horizontal) radius of influence was 125 (750) m. This elliptical volume of influence reduced the contamination of data from dynamically distinct layers above and below the level of interest.

Dual-Doppler synthesis and vertical integration were then performed using CEDRIC. Prior to the synthesis of a 2D wind field, the data at levels above 3000 m MSL were thresholded on the octant field to remove interpolation errors produced by the horizontal spacing of data points in the spherical coordinate system. Synthesis was performed using the two-equation method. Terminal fall speed velocities were determined by an inferred relationship to maximum reflectivity (Atlas et al. 1973), and a density correction was applied following the technique of Foote and du Toit (1969). The horizontal wind field was smoothed with a Leise two-step filter and patcher function in CEDRIC.

A variational scheme (upward/downward) was used in the vertical integration of the convergence field to determine vertical velocities. The lower boundary condition was calculated by determining the upslope component of the horizontal wind ($w = \mathbf{V}\cdot\nabla h$), with the elevation of the underlying topography (h) based on a 30 arc second digital terrain dataset. The upper boundary condition was set to zero. The most significant source of potential error is the integration scheme, for there is great uncertainty in the upper boundary condition caused by undersampling and a lack of dynamic knowledge. However, the vertical velocity analyses were examined primarily near the terrain, where the $\mathbf{V}\cdot\nabla h$ component dominated.

Radar reflectivities were based on data collected by the Promontory Point Weather Surveillance Radar-1988 Doppler (KMTX WSR-88D) on top of Promontory Point (see Fig. 1a for location) and the NOAA WP-3D X-band tail radar. KMTX provided high-frequency reflectivity analyses covering a broad region, whereas the WP-3D tail-mounted radar featured higher-resolution data within 20 km of the flight track and in low-elevation regions that were not sampled by KMTX because of overshooting or terrain blockage. KMTX level-II data (Crum et al. 1993) were interpolated to a Cartesian grid and are presented for a horizontal level near midmountain (2265 m). The WP-3D tail-radar data were also interpolated to a Cartesian grid and are provided for a horizontal level near the Wasatch Crest (2640 m MSL) and along a vertical cross section just south of the flight track and perpendicular to the Wasatch Mountains.

3. IOP3 structure and evolution

The 6-h period encompassing the most detailed observations (i.e., DOW and WP-3D) collected during IOP3 (1800 UTC 12 Feb–0000 UTC 13 Feb 2000) featured the passage of a midlevel (700–550 hPa) trough axis followed 3 h later by a surface-based trough passage. Cross-barrier winds supported orographic precipitation throughout the period. Ahead of the midlevel trough axis, southwesterly crest-level flow was observed over northern Utah. With crest-level winds featuring a substantial cross-barrier component, orographic precipitation enhancement was observed along the entire Wasatch Crest (Fig. 2a). In the Wasatch Mountains near OGD, the primary target area of IOP3, precipitation near the crest was roughly double that observed in the lowlands immediately upstream. To the lee, precipitation decreased by about a factor of 2 within 10–15 km of the crest. Precipitation observations also revealed that precipitation enhancement began upwind of the initial Wasatch slope, with the snow water equivalent (SWE) increasing from 0.23 cm at Hat Island (HAT), 70 km upstream of the crest, to 1.0 cm at OGD, 12 km upstream of the crest (Fig. 2b; Table 1). The most precipitation (2.3 cm SWE) was observed at the high-elevation (2438 m) Ben Lomond snowpack telemetry (SNOTEL) site (BLPU1), just north of the flight track (see Fig. 1b for location).

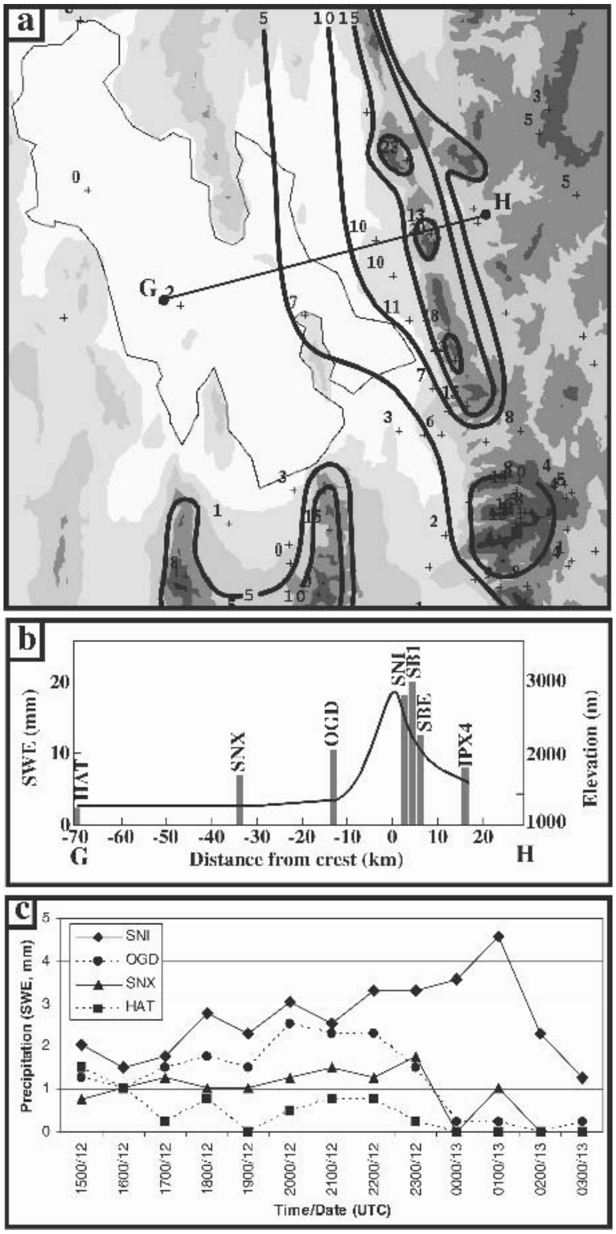

FIG. 2. Observed precipitation (SWE, mm) for selected periods during IOP3. (a) Accumulated precipitation over northern Utah from 1800 UTC 12 Feb to 0000 UTC 13 Feb 2000. (b) Accumulated precipitation observed by stations near line G–H of (a) from 1800 UTC 12 Feb to 0000 UTC 13 Feb 2000. Topography represented by solid line. (c) Hourly precipitation from selected stations near line G–H from 1500 UTC 12 Feb to 0300 UTC 13 Feb 2000. See Fig. 1 for station locations.

Hourly precipitation observations further emphasized the increase in precipitation as one approached and moved over the Wasatch Crest (Fig. 2c), but also showed that precipitation rates in the immediate upstream lowlands (OGD) approached those near the crest (SNI) from 2000–2200 UTC. Precipitation rates near the crest (SNI) continued to increase after 2200

TABLE 1. Precipitation station characteristics and accumulation (1800–0000 UTC).

Station	ID	Elevation (m)	Operating group	Gauge type	SWE (mm)
Hat Island	HAT	1293	University of Utah	ETI antifreeze weighing gauge	2
Antelope Island	SNX	1280	University of Utah	ETI antifreeze weighing gauge	7
Ogden	OGD	1362	National Weather Service	ASOS* heated tipping bucket	10
Snowbasin–Middle Bowl	SNI	2256	Snowbasin ski area	ETI antifreeze weighing gauge	18
Snowbasin–Strawberry Base	SB1	2000	Snowbasin ski area	ETI antifreeze weighing gauge	20
Snowbasin–Base	SBE	1925	University of Utah	ETI antifreeze weighing gauge	12
Ben Lomond	BLPU1	2438	Soil Conservation Service	SNOTEL pillow	23
Huntsville	IPX4	1550	University of Utah	Unheated weighing gauge	17

* ASOS is Automated Surface Observing System.

2300 UTC, while those in the lowlands decreased. While this was partially the result of the persistence of the storm over the Wasatch Mountains, it may also have been related to a delay in precipitation being measured at SNI. The Electronic Techniques, Inc. (ETI) weighing gauges used at SNI and other mountain sites beneath the flight track (e.g., SB1 and SBE, Table 1) use antifreeze to melt incoming snow and occasionally experience slush or snow buildup on the gauge walls. Such a buildup can delay the recording of precipitation as the snow must fall into the antifreeze mixture at the bottom of the gauge to be recorded.

We now examine the processes contributing to the precipitation distribution described above, with an emphasis on the kinematic and reflectivity structures upwind of, over, and to the immediate lee of the Wasatch Mountains. To facilitate our description, the section is organized around the four multilevel flight stacks that were executed by the NOAA WP-3D. Since flight stacks 1 and 2 were kinematically similar, the latter is not presented.

a. Flight stack 1

At 1735 UTC a forward-sloping midlevel (700–550 hPa) trough, which was accompanied by only a weak contrast in temperature and moisture (as indicated by the θ_{ei} analysis), was located over the Great Salt Lake ~80 km upstream of the Wasatch Crest (Fig. 3). As this feature gradually moved eastward, southwesterly crest-level flow impinged on the Wasatch Mountains, and radar reflectivities collected by KMTX and the NOAA WP-3D tail-mounted Doppler radar (~1830 UTC) showed high (>20 dBZ) reflectivities over and upstream of the Wasatch Mountains (Fig. 4). Reflectivity maxima were also found near Promontory Point and in a band that extended east-northeastward from Stansbury Island (the Stansbury band; Fig. 4a). The higher-resolution WP-3D tail-mounted Doppler radar revealed isolated reflectivity maxima directly over the highest peaks of the Wasatch, with the highest reflectivities over Ben Lomond Peak (BLP; Fig. 4b). Consistent with the aforementioned precipitation distribution, a broad region of weaker, but still significant reflectivities (>12 dBZ) extended over the lowlands to about 45 km upstream of the Wasatch Crest. Here, a radar cross section taken perpendicular to the Wasatch Mountain near OGD identified a pronounced reflectivity wall, characterized by vertically oriented isoechoes (Fig. 4c; see Fig. 4b for cross-section location). The highest reflectivities within this windward precipitation region

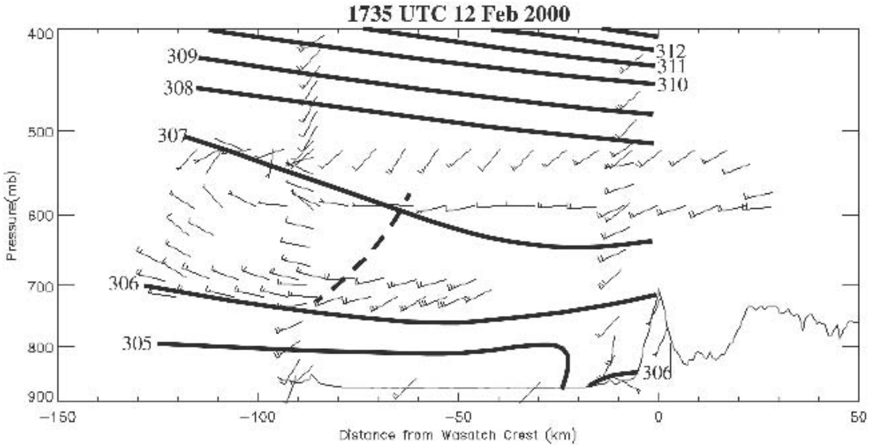

FIG. 3. Time–space-adjusted cross section of wind (full and half barbs denote 5 and 2.5 m s^{-1}, respectively) and θ_{ei} (every 1 K windward of crest) along line A–B of Fig. 1a at 1735 UTC 12 Feb 2000. Terrain profile denoted by thin line. Midlevel trough axis identified with thick dashed line.

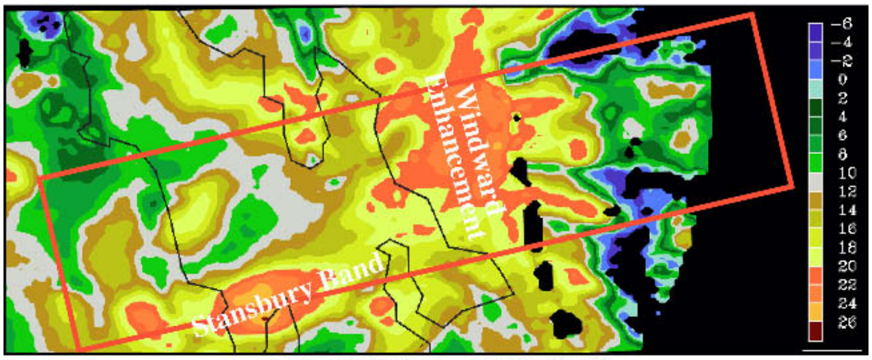

a) KMTX (2265 m, 1830 UTC)

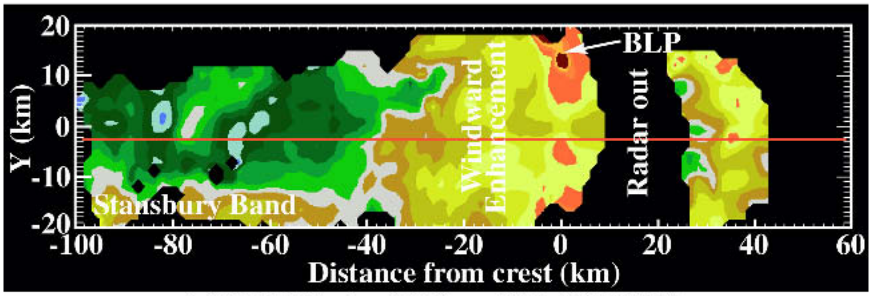

b) P3 Tail Radar (2640 m, 1817–1835 UTC)

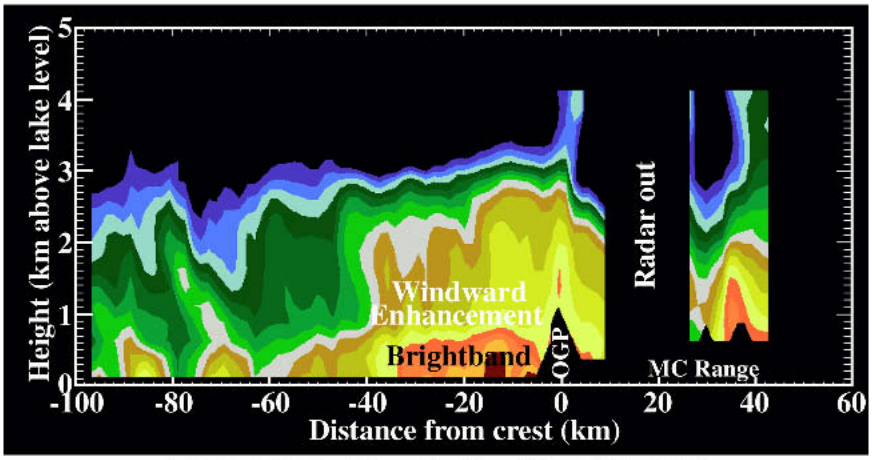

c) P3 Tail Radar Cross Section (1817–1835 UTC)

FIG. 4. (a) KMTX reflectivity (2265 m MSL) at 1830 UTC 12 Feb 2000. (b) WP-3D tail-mounted radar reflectivity (2640 m MSL) collected from 1817 to 1835 UTC 12 Feb 2000 [location denoted by red box in (a)]. (c) Barrier-normal WP-3D tail-mounted radar reflectivity cross section along red line indicated in (b). Reflectivity scale on right edge of (a).

were found near the ground and appeared to be the result of brightband contamination since they were at or below the 0°C level. A narrow, vertically oriented reflectivity maximum was located directly over the Wasatch Mountains where precipitation was heaviest. Aspects of the leeside reflectivity structure could not be examined during this flight leg due to a temporary radar outage.

MesoWest observations revealed that the reflectivity wall and windward precipitation region were located over and downstream of a low-level confluence between the southwesterly flow over the Great Salt Lake and the along-barrier southerly flow near the Wasatch Mountains (Fig. 5a). Analyses by a high-resolution data assimilation system run at the University of Utah (Lazarus et al. 2002) revealed that this confluence zone was convergent (not shown), and it will hereafter be termed a *windward convergence zone*.

To examine the possibility that topographic blocking was responsible for the windward convergence zone

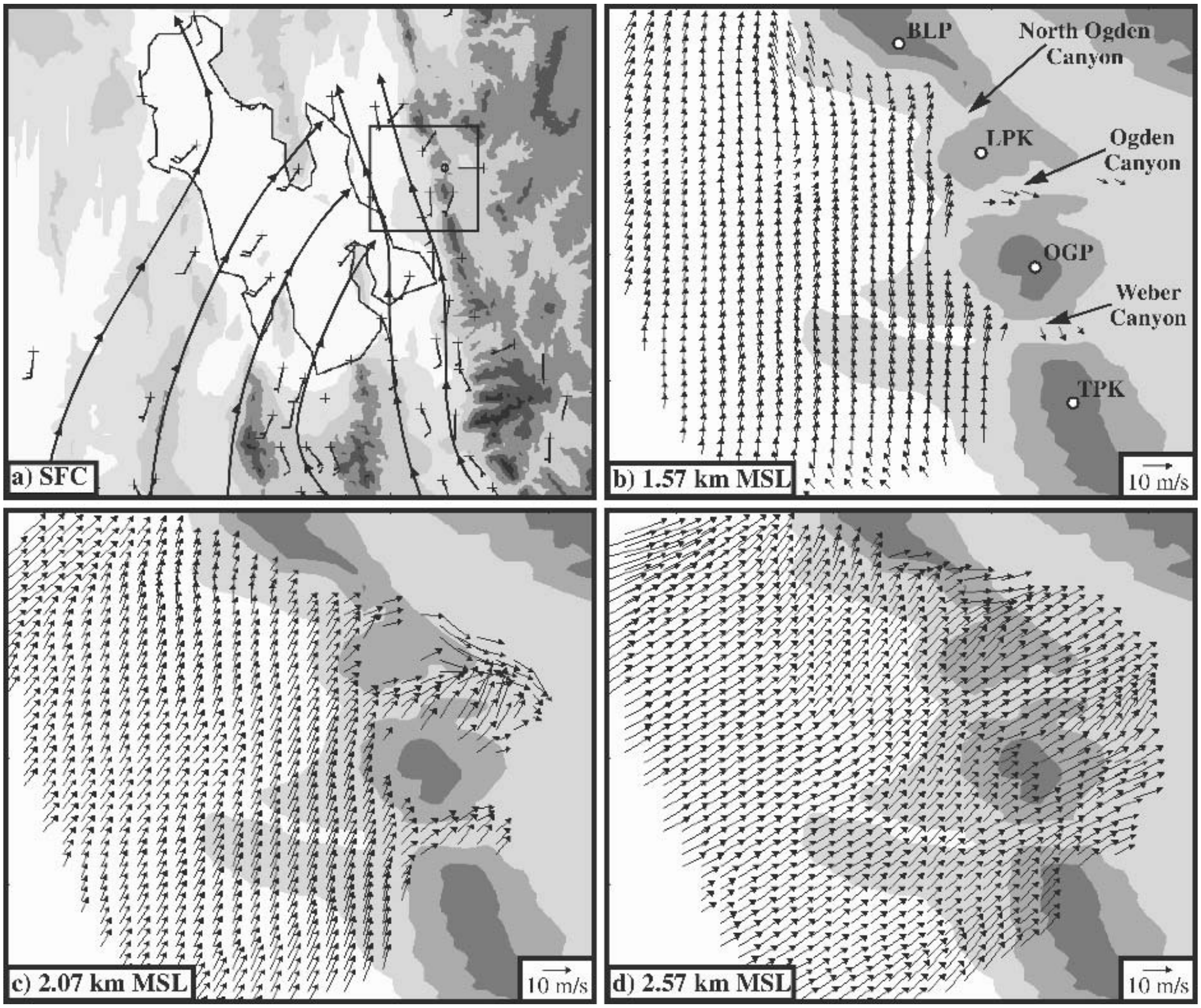

FIG. 5. (a) Manual streamline analysis at 1800 UTC 12 Feb 2000. Full and half barbs denote 5 and 2.5 m s^{-1}, respectively. Terrain shading as in Fig. 1. (b) The 1.57-km MSL DOW dual-Doppler wind analysis at 1832 UTC 22 Feb 2000. Vector scale at lower right. Terrain shading and location identifiers as in Fig. 1. (c), (d) Same as (b) except at 2.07 and 2.57 km MSL, respectively.

and precipitation enhancement, upper-air data collected by the NSSL mobile labs 100 km upstream and near the base of the Wasatch Mountains (LMR and OGD, respectively; see Fig. 1a for locations) just prior to the start of flight stack 1 (1735 UTC) are presented in Fig. 6. Potential temperature (θ) profiles showed that, with the exception of a shallow dry adiabatic layer near the surface at OGD, the atmosphere was absolutely stable to dry motion at both locations (Fig. 6a). However, small dewpoint depressions (0°–3°C) were observed at LMR and water (ice) saturated conditions were present at OGD below 600 (500) hPa. As a result, saturated parcel displacements were likely and may have also involved latent heat release associated with freezing. At LMR, the θ_{ei} decreased with height in a shallow layer near the surface (below ~840 hPa), then increased with height to ~810 hPa (Fig. 6a). Above 810 hPa, θ_{ei} was nearly constant with height. Thus, the upstream atmosphere was only weakly stable or neutral for saturated flow. At OGD, the θ_{ei} profile above 820 hPa was similar to that upstream, although the θ_{ei} was slightly higher. Below 820 hPa, the θ_{ei} was as much as 2 K greater than at LMR and a moist absolutely unstable layer (MAUL; Bryan and Fritsch 2000) was present between 840 and 820 hPa where dry-adiabatic lapse rates were observed despite the presence of saturation (see the θ profile in Fig. 6a; moisture profile not shown). Since the MAUL was located directly below the 0°C level, we hypothesize that it was produced by the diabatic cooling associated with melting snow. Compared to the upwind sounding site (LMR), θ and θ_{ei} were slightly higher at the near-barrier site (OGD). Although limited data prevented detailed analysis, low-level θ_{ei} varied by <1 K within 100 km of the Wasatch,

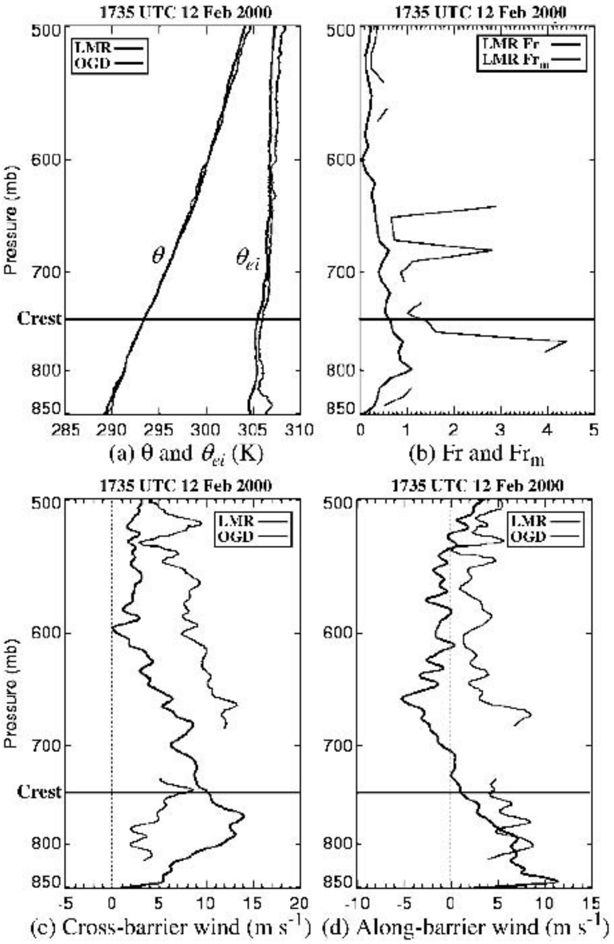

FIG. 6. Vertical profiles of (a) potential temperature (θ) and equivalent potential temperature with respect to ice (θ_{ei}) at LMR (black) and OGD (gray), (b) Froude number (Fr, black) and moist Froude number (Fr_m, gray) at LMR, (c) cross-barrier wind component at LMR (black) and OGD (gray), and (d) along-barrier wind component from LMR (black) and OGD (gray) at 1735 UTC 12 Feb 2000. Missing wind data at OGD not plotted. Elevation of Wasatch Crest indicated by horizontal line. The Fr_m profile is not plotted in layers where $N_m^2 \leq 0$.

as illustrated by the 1735 UTC cross section (Fig. 3). Therefore, a well-defined near-barrier cold pool was not apparent during this flight stack.

Figure 6b presents vertical profiles of the Froude number, $Fr = U/hN$ (where U is the cross-barrier flow component, N is the Brunt–Väisälä frequency, and h is the height of the barrier), and moist Froude number, $Fr_m = U/hN_m$ [where N_m is the saturated Brunt–Väisälä frequency calculated following Durran and Klemp (1982)] from the upstream sounding site (LMR). The barrier height, h, was set to 1300 m, roughly the difference between the elevation of the Great Salt Lake and the Wasatch Crest near OGD (excluding major passes). We found that Fr was less than one at all levels except 800 hPa and was less than 0.5 below 825 hPa. Although this appears to be a favorable situation for blocking (i.e., $F_r < 1$), the flow was likely characterized by saturated motion and Fr_m was >1 or indeterminate (i.e., $N_m^2 < 1$) throughout most of the atmosphere below crest level. The only layer below crest level where Fr_m was <1 was between 840 and 820 hPa. Thus, the potential for blocking was likely limited and confined to below about 820 hPa (i.e., midmountain). While Fr_m was not calculated with respect to ice processes, it can be inferred qualitatively that the latent heat of fusion would further decrease the static stability and the potential for blocking.

Profiles of cross-barrier wind speed did reveal a weaker cross-barrier flow component near the barrier below crest level. Upstream, at LMR, the cross-barrier wind at all levels except the surface ranged from 5–14 m s^{-1}, with a maximum just below crest level (Fig. 6c). In contrast, at OGD, the cross-barrier wind component was 6 m s^{-1} or less (winds at the lowest levels were not available because of a balloon-tracking problem). The along-barrier wind component below crest level, however, was also larger at LMR than OGD (Fig. 6d). Thus, although the flow was predominantly along-barrier at OGD, there was no acceleration of the along-barrier flow near the barrier. In contrast, studies of blocked flow or cold-air damming have typically observed an enhancement of the along-barrier flow (e.g., Parish 1982; Dunn 1987; Bell and Bosart 1988; Overland and Bond 1995). The lack of a well-defined near-barrier cold pool also differs from earlier studies. Thus, the processes responsible for the development of the windward convergence zone appear to be more complex than described by prior studies, as discussed in section 4.

Figures 5b–d illustrate the near-barrier flow field between the convergence zone and the Wasatch Mountains at 1832 UTC. The levels presented are 1565 m MSL (300 m above lake level), 2065 m MSL (midmountain), and 2565 m MSL (near crest level). The low-level flow was generally southerly and along barrier, although there was a somewhat stronger cross-barrier flow component at the extreme western edge of the dual-Doppler lobe (Fig. 5b). Near BLP, where the largest reflectivities were observed, the southerly flow was deflected westward where it converged with a southerly-to-southwesterly flow to the west.

At midmountain, the flow was generally south-southwesterly to southwesterly, with a significant cross-barrier component upstream of the highest terrain features where the highest reflectivities were observed (Fig. 5c; see also Fig. 4). Flow deflection and splitting were evident upstream of Lewis (LPK) and Ogden Peaks (OGP), and strong upcanyon flow was found in Weber, Ogden, and North Ogden Canyons. Near crest level, winds were generally southwesterly, with a similar pattern of flow splitting evident over the highest peaks (Fig. 5d).

Figure 7 presents the along- and cross-barrier flow components normal (C–D; see Fig. 1b) and parallel

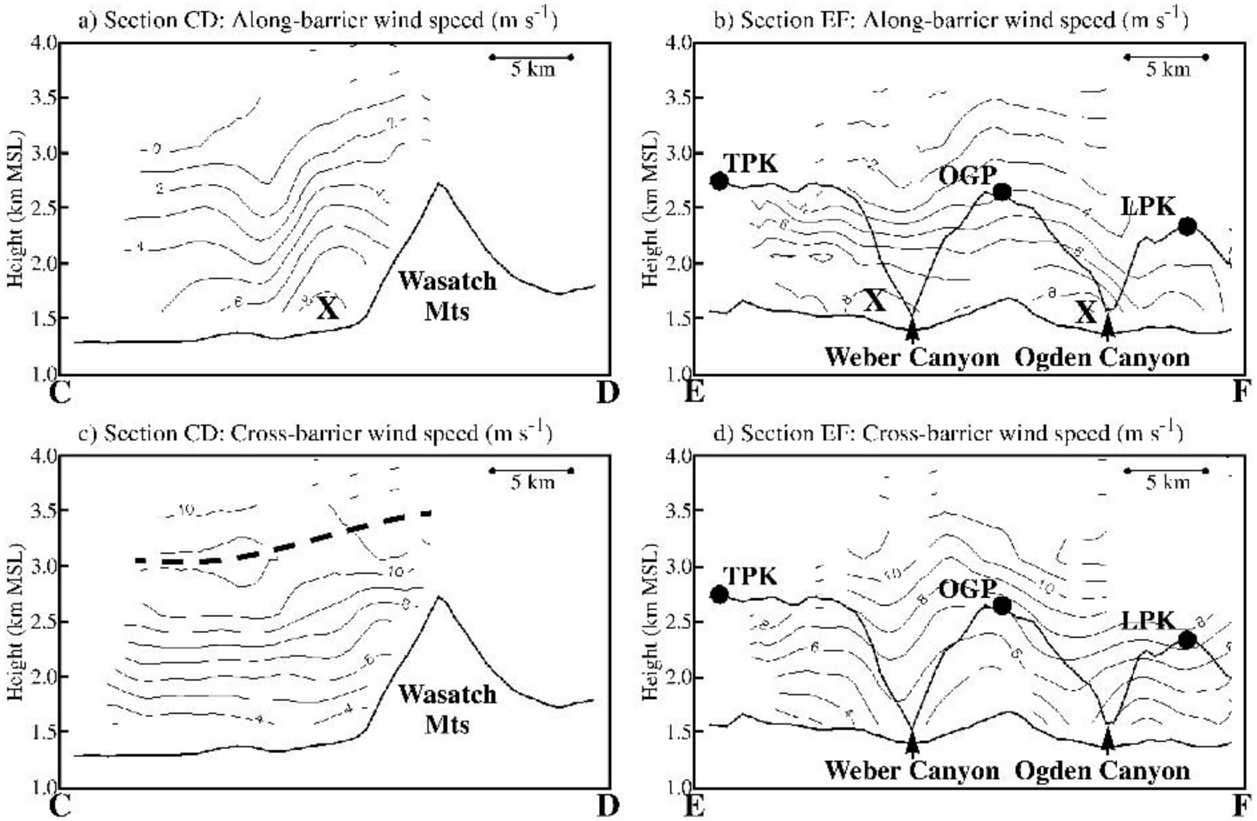

FIG. 7. Cross sections of along-barrier and cross-barrier winds at 1832 UTC 12 Feb 2000. (a) Along-barrier winds in ridge-normal cross section C–D (contours every 1 m s^{-1} with maximum indicated by X). (b) Along-barrier winds in ridge-parallel cross section E–F [contours and maxima as in (a)]. (c) Cross-barrier winds in ridge-normal cross section C–D (contours every 1 m s^{-1} with level of maximum cross-barrier flow indicated by dashed line). (d) Cross-barrier winds in ridge-parallel cross section E–F (contours every 1 m s^{-1}). Outline of Wasatch Crest east of the cross section E–F is identified by gray line in (c) and (d). Major topographic features annotated.

(E–F) to the main axis of the Wasatch ridgeline (henceforth ridge normal and ridge parallel, respectively). The ridge-normal cross section (C–D) showed a shallow 8 m s^{-1} along-barrier flow maximum near the base of the Wasatch Mountains (Fig. 7a). The along-barrier flow weakened to near zero at 3–3.5 km MSL and its depth increased toward the barrier. Although the along-barrier flow maximum qualitatively resembled barrier jets observed along the Sierra Nevada (Parish 1982), Colorado Front Range (Dunn 1992), and coastal terrain of western North America (Overland and Bond 1995), it was smaller in horizontal scale. The ridge-parallel cross section (E–F) revealed that the along-barrier flow featured near-surface maxima just upstream (south) of the major canyons (Fig. 7b). These maxima appeared to be related to flow accelerations just to the lee of relatively low amplitude topographic benches in the lowlands upstream of the Wasatch (somewhat evident in the thick black surface contour in Fig. 7b and terrain shading in Figs. 5b–d).

The cross-barrier flow along ridge-normal cross section (C–D) increased with height from less than 4 m s^{-1} at the lowest levels to an 11 m s^{-1} maximum that sloped upward toward the barrier and over the crest (Fig. 7c). The ridge-parallel cross section (E–F) revealed enhanced cross-barrier flow entering the major canyons, particularly Weber Canyon (Fig. 7d).

Flight-level vertical velocity traces collected by the NOAA WP-3D are presented in Fig. 8. At upper levels (5274 and 4348 m MSL), the vertical velocity was near zero or positive well removed from the crest, with the wavelike structure, combined with the near-neutral moist stability, suggesting the presence of embedded convection (Figs. 8a,b). At 4348 m, the ascent became stronger over the windward convergence zone and precipitation region. Trapped lee waves were found downstream of the Wasatch Crest and were strongest (~1 m s^{-1}) immediately to the lee of the barrier. Scorer parameter profiles (not shown) indicated favorable conditions for trapped lee waves at these levels. At lower levels (3124 and 2817 m MSL, flight legs terminated upwind of the barrier because of terrain-based flight restrictions), the amplitude of vertical velocity fluctuations within about 40 km of the barrier, roughly the position of the windward convergence zone and reflectivity wall, was much larger than aloft (Figs. 8c,e).

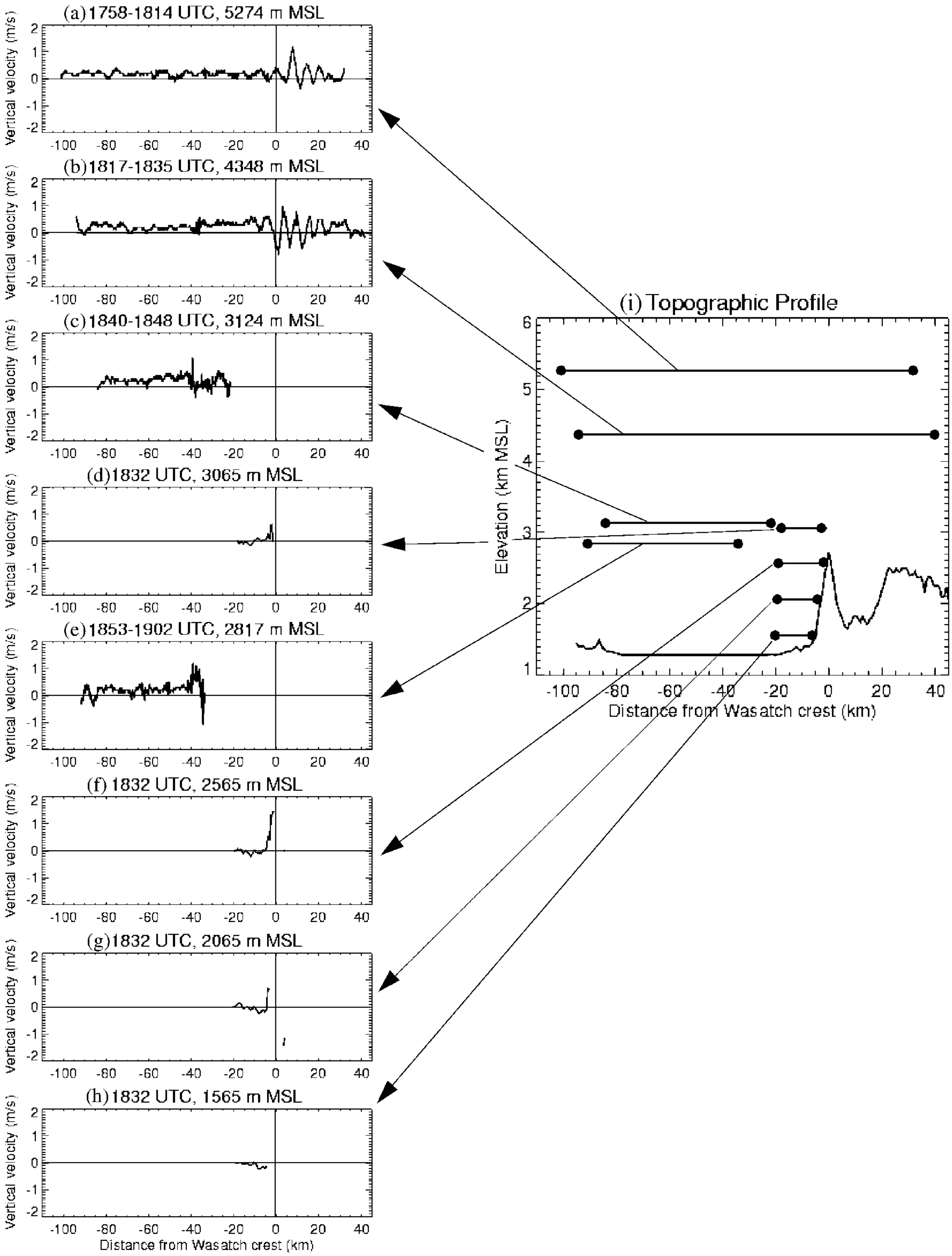

FIG. 8. NOAA WP-3D flight-level and DOW-derived vertical velocities (*w*) during stack 1 (1758–1902 UTC 12 Feb 2000). (a) WP-3D *w* at 5274 m MSL. (b) WP-3D *w* at 4348 m MSL. (c) WP-3D *w* at 3124 m MSL. (d) DOW-derived *w* at 3065 m MSL. (e) WP-3D *w* at 2817 m MSL. (f) DOW-derived *w* at 2565 m MSL. (g) DOW-derived *w* at 2065 m MSL. (h) DOW-derived *w* at 1565 m MSL. (i) Topography along transect with vertical velocity levels annotated. Legs (c) and (e) are truncated because of terrain-based flight restrictions.

At lower levels near the barrier, DOW-derived vertical velocities revealed strong upward motion (0.5–1.5 m s^{-1}) within about 5 km of the mid- (2065 m MSL) and upper-elevation (2565 m MSL) windward slope of the Wasatch (Figs. 8f,g). This vertical motion is consistent with the interaction of the 6–8 m s^{-1} mid-to-upper-mountain cross-barrier flow, with the windward slope of the Wasatch (see Fig. 7a) and the localized reflectivity maxima found over the highest peaks (Fig. 4). Weaker upward motion at 3065 m (Fig. 8d) suggests that this intense vertical motion was limited to very near the mid-to-upper-mountain elevations where a strong upslope component of the horizontal wind was observed (e.g., Fig. 5). At lower elevations (1565 m MSL), where the flow was mainly ridge parallel, weak vertical motion was observed (Fig. 8h).

In summary, flight stack 1 featured two pronounced orographic precipitation features. The first was a region of enhanced precipitation that extended over the lowlands to 40 km upstream of the Wasatch Crest. This feature was collocated with a low-level convergence between the southwesterly flow over the Great Salt Lake and the along-barrier southerly flow near the Wasatch Mountains. The second was a narrow region of precipitation enhancement that was located directly over the crest. This region of enhancement appeared to be produced by a narrow zone of intense vertical motion that was located within about 5 km of the mid-to-upper-elevation windward slopes of the Wasatch. The overall flow pattern near the barrier was characterized by nearly along-barrier flow at low levels veering to cross-barrier at crest level. Smaller-scale orographic circulations included flow splitting upwind of major peaks and channeled flow in major canyons. Although many aspects of the flow pattern were consistent with topographic blocking, such as a decrease in the magnitude of the cross-barrier flow at low levels, other aspects were inconsistent, including the lack of a well-defined near-barrier cold pool, as discussed in more detail in section 4.

b. Flight stack 3

By 2035 UTC the midlevel trough axis was located over and immediately upstream of the Wasatch Mountains and adjoining lowlands (Fig. 9). Precipitation rates increased over the immediate upstream lowlands as this feature approached and moved overhead (e.g., OGD from 2000–2200 UTC; Fig. 2c) and dramatic changes occurred in both kinematic and reflectivity structure. KMTX radar imagery from 2110 UTC showed the highest reflectivities over and immediately upstream of the Wasatch Mountains (Fig. 10a). Isolated reflectivity maxima were observed by the WP-3D tail-mounted radar over the highest peaks of the Wasatch (Fig. 10b). These orographic reflectivity maxima were similar in scale, but greater in magnitude, to those observed during flight stack 1 (cf. Figs. 4b, 10b). The windward precipitation region extended about 25 km upstream from the Wasatch Mountains with the reflectivity wall located 15 km closer to the crest than observed during flight stack 1 (cf. Figs. 4c, 10c). Thus, the windward precipitation region collapsed toward the Wasatch Mountains during the passage of the midlevel trough. Additional mesoscale precipitation features included the Stansbury band, which extended 50 km upstream of the barrier just south of Antelope Island (SNX; see Fig. 1 for location), and a transient precipitation band, 40–60 km upstream of the Wasatch Crest, which extended from Promontory Point to near Stansbury Island (Fig. 10b).

To the lee of the Wasatch Mountains, the isoechos sloped strongly downward and the accompanying re-

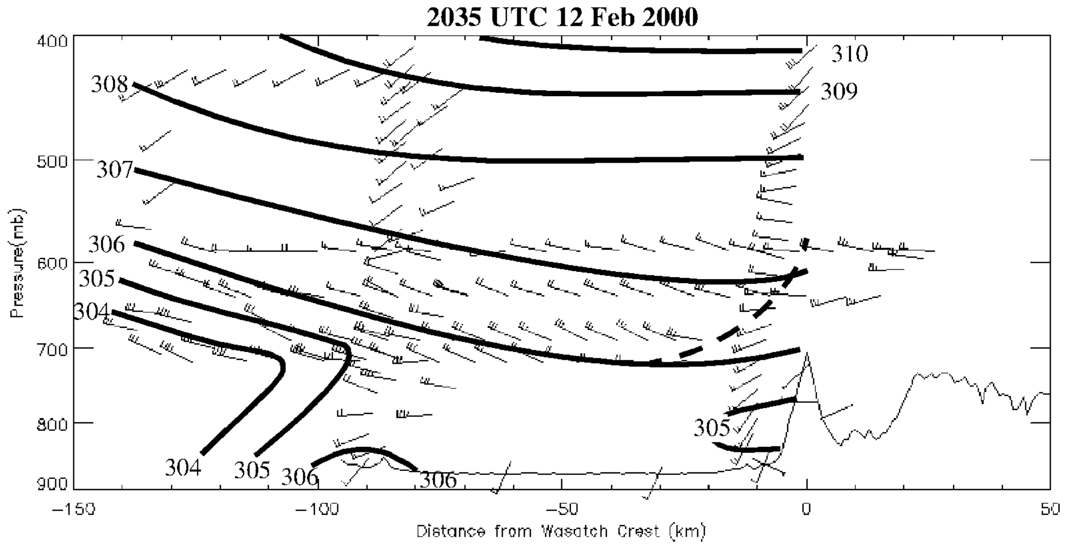

FIG. 9. Same as Fig. 3 except for 2035 UTC 12 Feb.

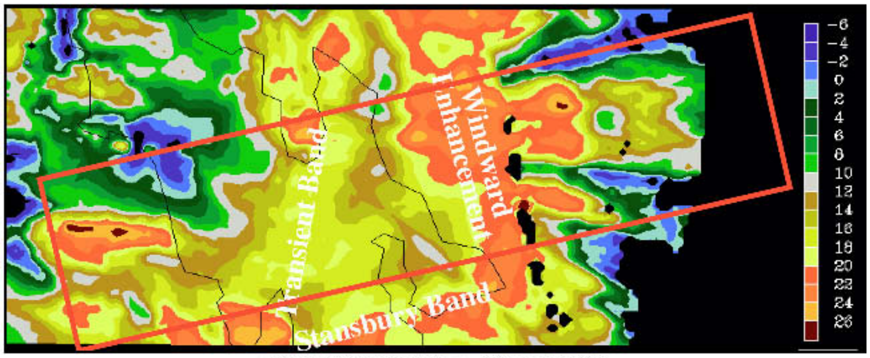

a) KMTX (2265 m, 2110 UTC)

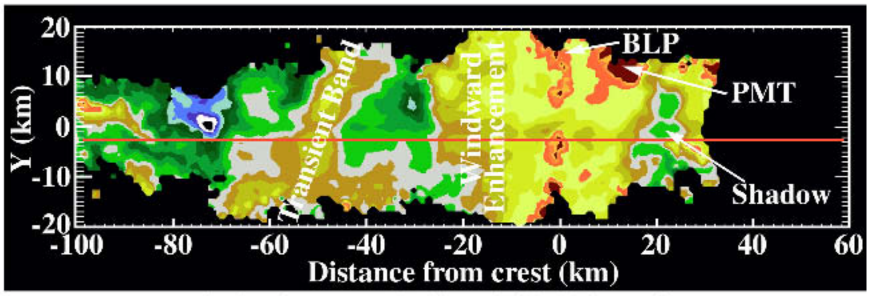

b) P3 Tail Radar (2640 m, 2110–2127 UTC)

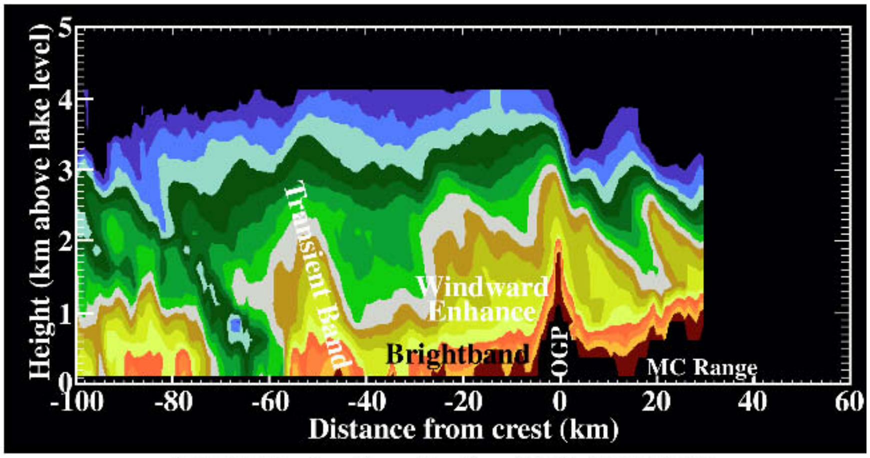

c) P3 Tail Radar Cross Section (2110–2127 UTC)

FIG. 10. Same as Fig. 4 except for (a) 2110 UTC 12 Feb 2000 and (b), (c) 2110–2127 UTC 12 Feb 2000.

flectivity minimum eventually intersected with the Monte Cristo Range, 20–25 km downstream of the Wasatch Crest (Fig. 10c; see Fig. 1a for location of Monte Cristo (MC) Range). Thus, the spillover of large hydrometeors aloft appeared to be limited.

Thermodynamic profiles collected by the NSSL mobile laboratories just prior to the start of stack 3 (2035 UTC) are presented in Fig. 11a. The θ profiles revealed that the atmosphere was statically stable for dry motion above both the surface-based mixed layer at LMR and a shallow surface-based superadiabatic layer at OGD. At LMR, θ_{ei} decreased or was constant with height through most layers below 700 hPa, a reflection of deepening low-level potential instability (cf. Figs. 6a, 11a). Near the barrier, at OGD, the potential instability was confined to below 775 hPa. At both sites, θ_{ei} increased very gradually with height farther aloft.

Unlike 3 h earlier, low-level (below 775 hPa) θ and θ_{ei} were lower near the barrier (OGD) than upstream (LMR; cf. Figs. 6a, 11a). The development of this near-barrier cold pool, which was also apparent in the time–space-adjusted cross section (Fig. 9), appeared to be the result of low-level diabatic processes. At LMR, where no precipitation was observed between the 1735 and

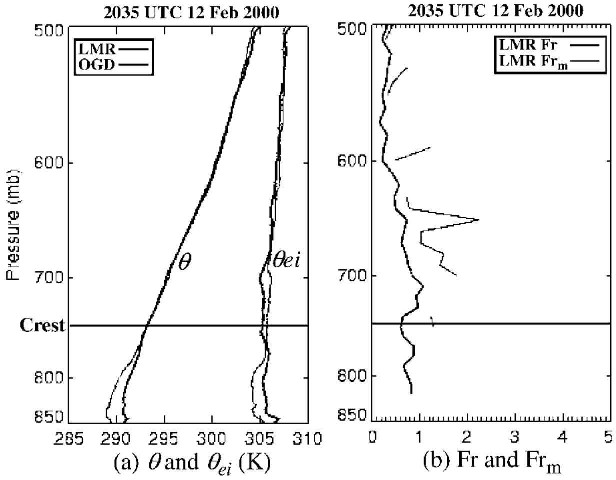

(a) θ and θ_{ei} (K) (b) Fr and Fr$_m$

FIG. 11. Same as Figs. 6a and 6b except for 2035 UTC 12 Feb 2000, there is no missing data, and Fr profile not plotted in layers where $N^2 \leq 0$.

2035 UTC soundings, diurnal surface heating, although limited by cloud cover, was able to increase the low-level θ and θ_{ei} and generate a shallow mixed layer (Fig. 11a). In contrast, at OGD, precipitation rates reached 2.3–2.5 mm h^{-1} during the 2-h period prior to and during sounding launch (not shown). Concurrently, surface θ_{ei} decreased steadily. Thus, we hypothesize that diabatic cooling associated with melting snowfall (e.g., Wexler et al. 1954; Marwitz and Toth 1993; Kain et al. 2000), which was distributed through the low levels by moist-convective mixing, was responsible for the development of the near-barrier cold pool. Evaporative cooling was likely limited since the atmosphere was saturated throughout the period.

Profiles of Fr and Fr$_m$ from the upstream sounding site (LMR) are presented in Fig. 11b. Between the well-mixed near-surface layer, where Fr was indeterminate, and crest level (~700 hPa), Fr ranged from 0.5 to 1.0, with smaller values farther aloft. We found that Fr$_m$ was indeterminate at all levels below 700 hPa, since lapse rates were near or greater than moist adiabatic. Compared with 3 h earlier (Fig. 11b), Fr and Fr$_m$ were higher or indeterminate in all layers except near 800 hPa, suggesting a decrease in the already limited potential for blocking.

Consistent with the decrease in blocking potential, southwesterly surface flow began to penetrate into the lowlands east of the Great Salt Lake (Fig. 12a). Concurrently, low-level convergence, the reflectivity wall, and the windward precipitation region collapsed toward the barrier. The low-level dual-Doppler wind analysis for 2110 UTC revealed that the along-barrier southerly flow had become confined to within 5 km of the slope of LPK and OGP (Fig. 12b). Farther upstream, the flow was transitioning to southwesterly. Midmountain winds had veered and strengthened since flight stack 1, and now featured a larger cross-barrier component (Fig. 12c). Confluent upcanyon flow also persisted at this level. To the north, the southwesterly crest-level flow was deflected eastward by BLP, which because of its unique orientation, was oriented more obliquely to the incident flow than the rest of the Wasatch Crest. The larger cross-barrier moisture flux arising from this unique orientation helps explain the higher reflectivities and greater precipitation that were observed over BLP. At crest level, the upstream flow exhibited weak cyclonic curvature as it approached the Wasatch (Fig. 12d). Since flight stack 1, the winds at this level had veered and increased in magnitude, resulting in a larger cross-barrier flow component (cf. Figs. 5d, 12d).

Decreases in both the strength and horizontal scale of the along-barrier flow were further illustrated by the ridge-normal cross section presented in Fig. 13a. The 6 m s^{-1} along-barrier wind maximum near the base of the Wasatch Mountains was 2 m s^{-1} weaker than that observed during flight stack 1 (cf. Figs. 7a, 13a). The along-barrier wind magnitude both upstream and aloft was also weaker, and the zero isotach had lowered to below crest level. In the ridge-parallel cross section (EF), the along-barrier flow was weaker at all locations (Fig. 13b). Consistent with the analysis during flight stack 1, the strongest along-barrier flow was found just south of Weber Canyon (cf. Figs. 7b, 13b) and may have been related to the interaction of the along-barrier flow with a topographic bench.

In the ridge-normal cross section (C–D), the cross-barrier wind speed maximum had lowered about 500 m while maintaining a similar magnitude (cf. Figs. 7c, 13c). The cross-barrier flow had also strengthened below this maximum as the terrain blocking weakened and the near-surface flow veered to southwesterly. The ridge-parallel cross section (E–F) showed that the strongest cross-barrier flow was located just above the crest with locally enhanced cross-barrier flow found near Weber Canyon, as was observed earlier (cf. Figs. 7d, 13d).

Vertical velocity traces from flight stack 3 are presented in Fig. 14. At upper levels (4363 and 3742 m), vertical velocities were generally positive with the amplitude of the wavelike oscillations within 40 km of the crest increasing near the barrier (Figs. 14a,b). At 4363 m, a narrow zone of intense subsidence (>1.5 m s^{-1}) associated with a lee wave was observed immediately downstream of the crest (Fig. 14a). This feature was somewhat weaker during the 3742-m flight leg (Fig. 14b). Downward advection of hydrometeors within the lee wave likely limited leeside spillover farther downwind, resulting in the strong downward slope of isoechoes to the lee of the barrier (Fig. 10c). At lower levels upstream of the Wasatch (3133 and 2823 m), the WP-3D vertical velocities showed considerable variability, although the mean vertical motion was positive (Figs. 14c,e). Near the barrier, the DOW-derived vertical motion showed strong (~1.5 m s^{-1}) ascent near the mid-

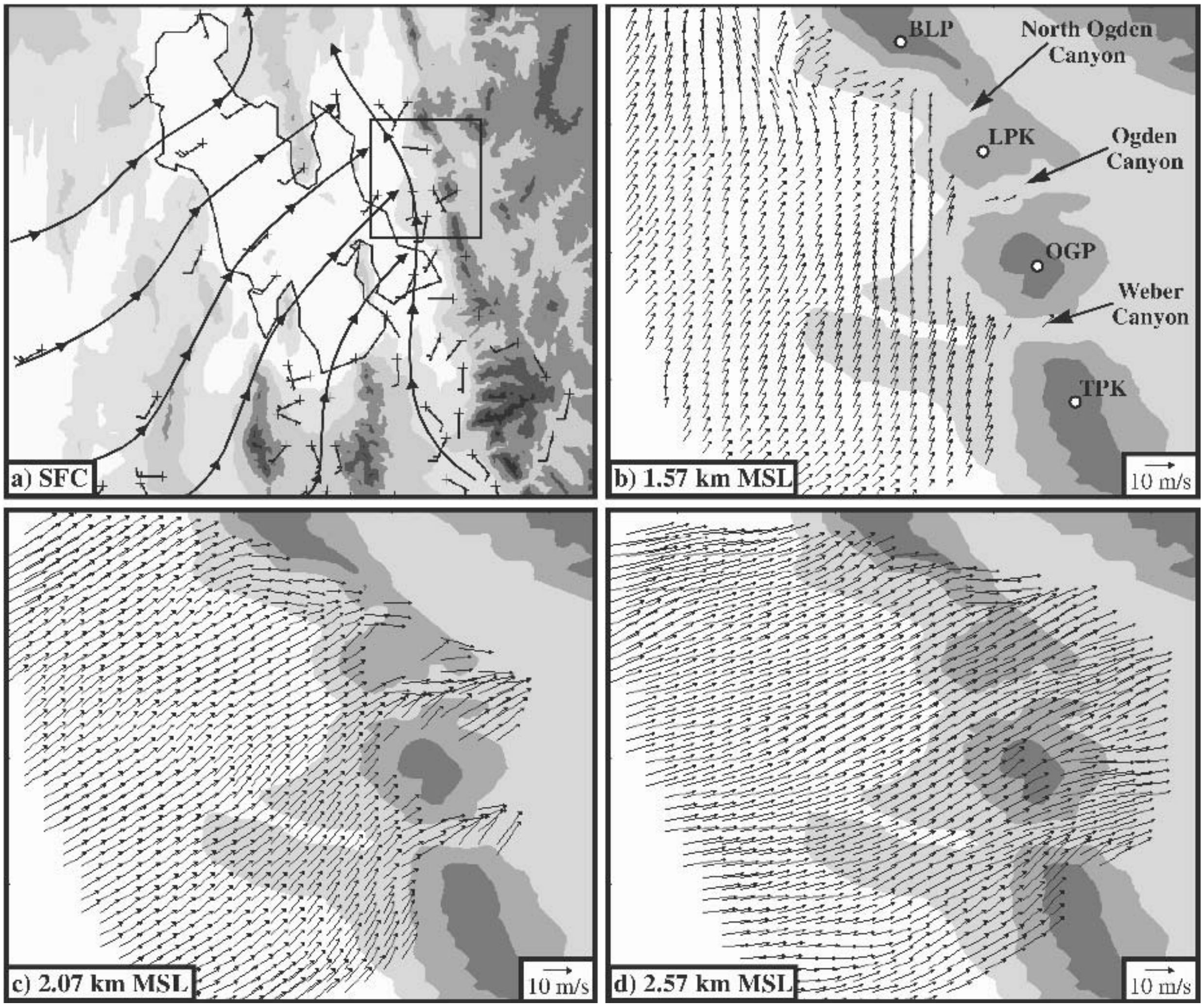

FIG. 12. Same as Fig. 5 except (a) manual streamline analysis is for 2100 UTC 12 Feb 2000 and (b)–(d) DOW dual-Doppler wind analyses are for 2110 UTC 12 Feb 2000.

mountain windward slope of the Wasatch Mountains, consistent with the strong cross-barrier flow (Fig. 14g). This was the only level where such strong ascent was evident (Figs. 14d,f,h), although the vertical velocity at 2656 and 3065 m could not be derived as close to the barrier as in flight stack 1.

In summary, the kinematic and precipitation structure of IOP3 underwent significant changes between flight stacks 1 and 3 as the midlevel trough moved across the Wasatch Crest. The along-barrier flow eroded and collapsed toward the Wasatch Mountains, with the along-barrier jet weakening and becoming increasingly confined both horizontally and vertically. The windward convergence zone and precipitation region also moved toward the barrier and were now located within 25 km of the crest. Similar to flight stack 1, narrow reflectivity maxima were found over the highest peaks of the Wasatch Mountains, although these maxima were stronger than observed previously, consistent with increased cross-barrier flow at crest level. Strong subsidence was observed in a lee wave and, based on the strong downward slope of reflectivity isoechoes near this feature, appeared to limit the spillover of hydrometeors aloft.

c. *Flight stack 4*

By flight stack 4, the midlevel trough axis was well downstream of the study region, and westerly-to-northwesterly flow dominated the midlevels [Fig. 15, time adjustment to the midpoint of the flight stack (2300 UTC) since mobile laboratory soundings were not available]. Three regions of heavy precipitation were observed by the KMTX radar at 2310 UTC (Fig. 16a). The first was over and immediately upstream of the Wasatch Mountains, the second was a broad precipitation band that was moving over the north arm of the Great Salt Lake, and the third was a convective line that was located just west of the Great Salt Lake and

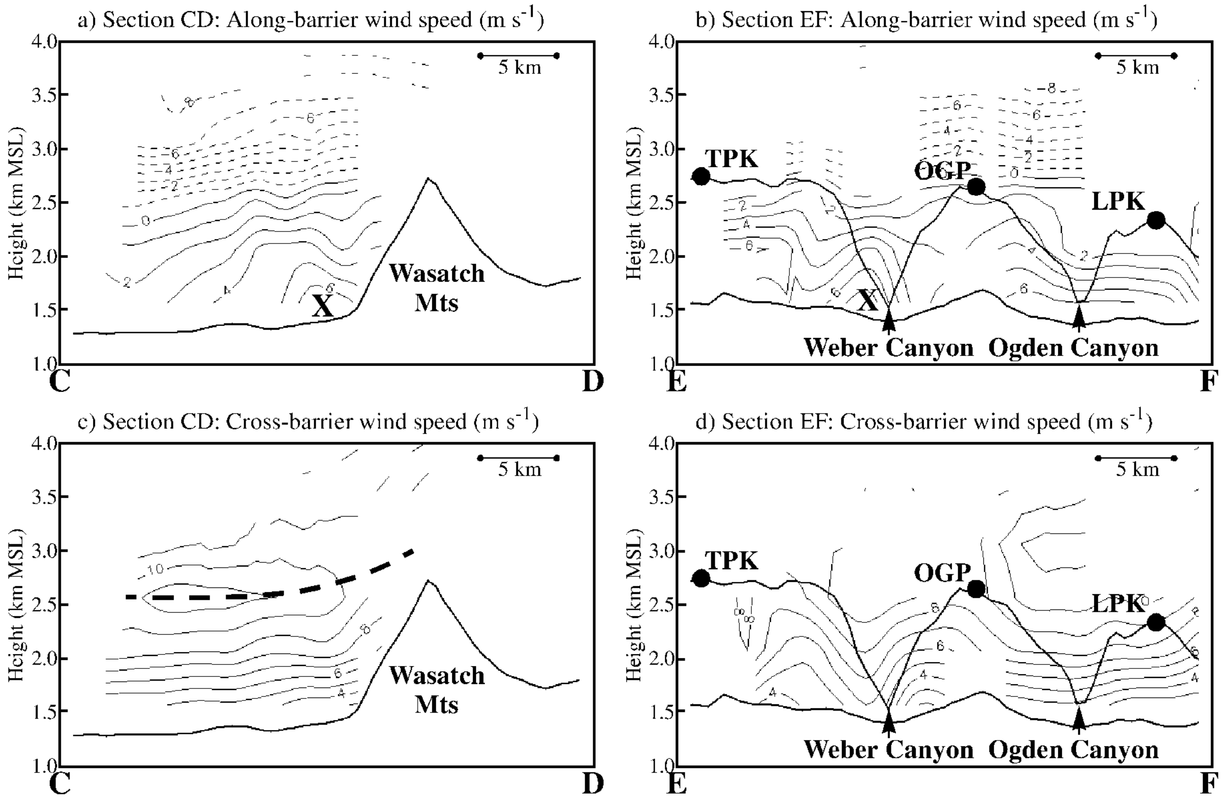

FIG. 13. Same as Fig. 7 except for 2110 UTC 12 Feb 2000 and negative contours dashed.

behind a surface pressure trough that was approaching from the west (Shafer 2002). Crest-level reflectivities collected by the NOAA WP-3D tail-mounted Doppler radar illustrated the persistence of heavy orographic precipitation near the Wasatch Crest, although it was confined to mainly beneath and south of the flight track (Fig. 16b). This region of heavy precipitation was also evident in the radar cross section (Fig. 16c). The windward precipitation region continued to become increasingly confined to near the barrier, and the reflectivity wall was now located only about 15 km upstream of the Wasatch Crest. A weak cold pool also persisted near the Wasatch Mountains (Fig. 15).

Although DOW data were unavailable for this flight stack, Meso West observations showed west-southwesterly flow penetrating across the entire southern half of the Great Salt Lake with a narrow zone of along-barrier flow persisting only very near the base of the Wasatch Mountains (Fig. 17). This continued narrowing and decay of the along-barrier flow occurred in concert with the collapse of the windward precipitation region toward the barrier. Farther upstream, winds shifted to northwesterly behind the convective line.

Upstream of the barrier, the vertical velocity traces for the lower-level flight tracks showed weak vertical motion, with some areas of subsidence (Figs. 18c,d), consistent with a trend toward large-scale subsidence in the post-midlevel trough environment. Aloft (4371 and 3753 m), the strongest (>2 m s^{-1}) lee waves of the event were observed (Figs. 18a,b).

In summary, the observations from flight stack 4 illustrate the continued collapse of the windward precipitation region toward the barrier. Along-barrier flow became increasingly confined to near the windward slope, where it persisted until the passage of the convective line at around 2300 UTC (not shown).

4. Discussion

a. A summary schematic

The relationship between the major kinematic and precipitation characteristics of IOP3 is summarized in Fig. 19. Low-level convergence between southwesterly flow over the Great Salt Lake and along-barrier flow near the Wasatch Mountains resulted in precipitation enhancement over the lowlands 30–40 km upstream of the Wasatch Crest. The windward convergence zone, along-barrier flow, and upstream precipitation region moved toward the barrier during and following the passage of a midlevel trough (evolution not shown). Meanwhile, at mid- and upper-mountain levels, southwesterly flow produced strong ascent within a few kilometers of the windward slopes that produced a localized

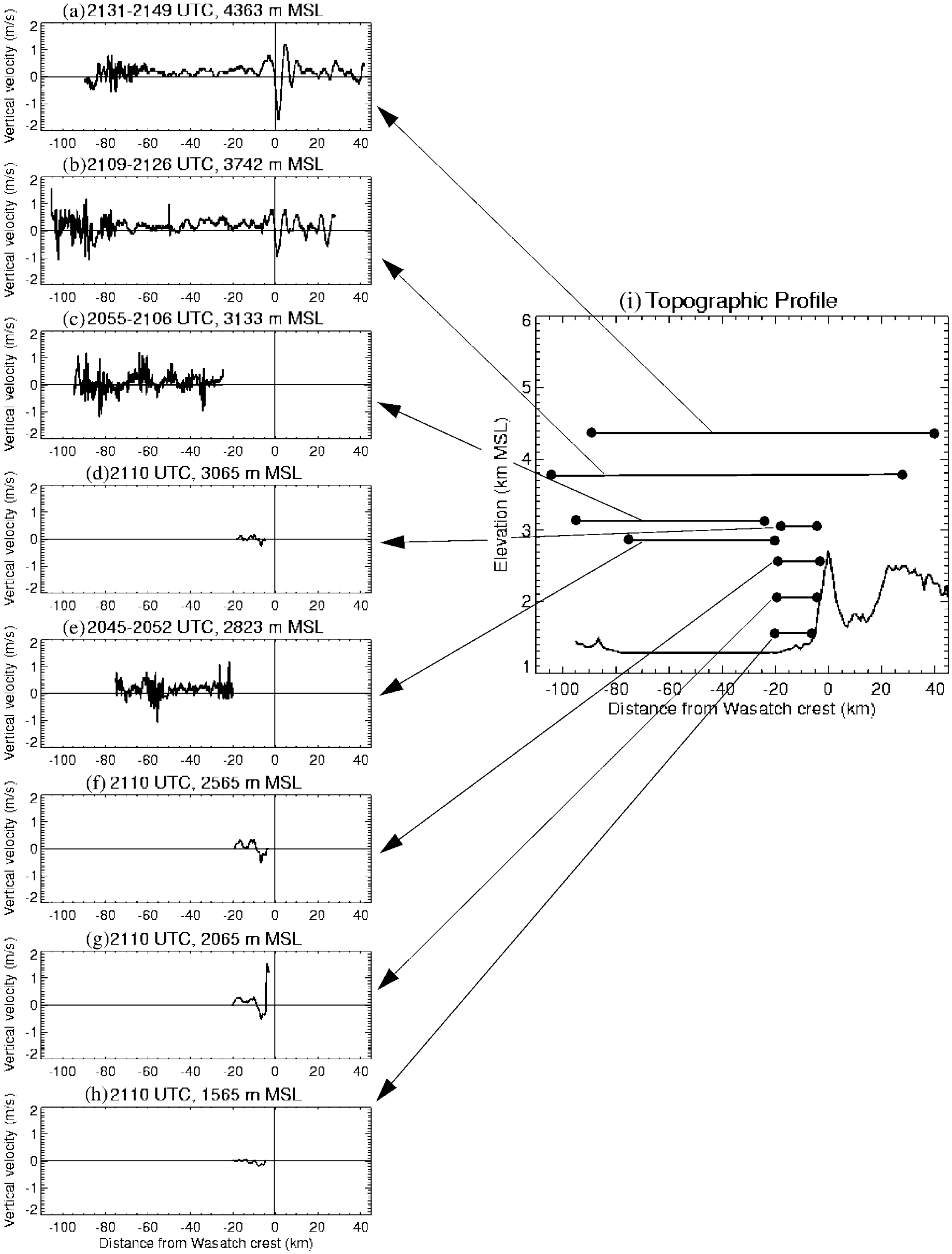

FIG. 14. Same as Fig. 8 except for stack 3 (2043–2228 UTC 12 Feb 2000) and 2110 UTC 12 Feb 2000 DOW analyses. Flight leg altitudes are (a) 4363, (b) 3742, (c) 3133, (d) 3065, and (e) 2823 m MSL, respectively.

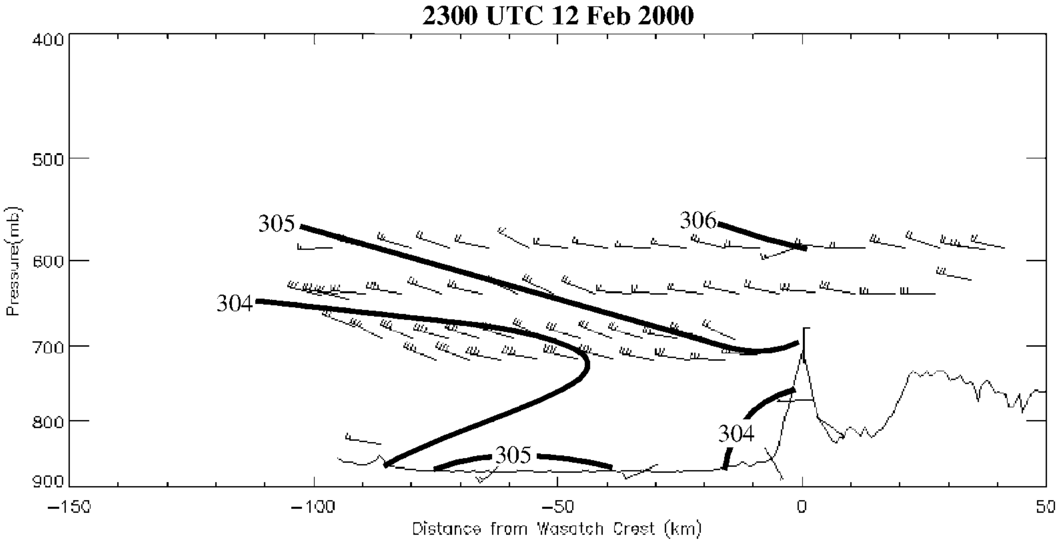

FIG. 15. Same as Fig. 3 except for 2300 UTC 12 Feb.

precipitation maximum over the Wasatch Crest. To the lee, mountain-wave-induced subsidence limited hydrometeor spillover aloft. Although not included in the schematic, the heaviest precipitation was observed on BLP, which, because of its unique orientation, was oriented more normal to the flow than the rest of the Wasatch Range.

b. Comparison with other orographic precipitation and blocking studies

Upstream precipitation enhancement similar to that illustrated in Fig. 19 has been observed near other mountain ranges. For example, Neiman et al. (2002) described how shallow, terrain-blocked flow enhances precipitation upstream of the coastal mountains of California and presented a conceptual model for blocked-flow events (their Fig. 19) that is similar to our Fig. 19. Peterson et al. (1991) used idealized numerical simulations to show that flow blocking upstream of the Park Range of Colorado results in enhanced upstream and slightly reduced crest-level precipitation compared with unblocked situations. Similarly, the distribution of precipitation over the Lago Maggiore region of the European Alps is modified by the degree of low-level blocking (e.g., Medina and Houze 2003).

The upstream precipitation enhancement during IPEX IOP3 contrasts with the aforementioned studies because it occurred with relatively weak static stability (i.e., near-moist-neutral saturated flow). There were also differences between IOP3 and more dramatic, blocked-flow events (e.g., Parish 1982; Dunn 1987, 1992; Marwitz 1987a; Bell and Bosart 1988; Colle and Mass 1995; Overland and Bond 1995; Braun et al. 1999; Bousquet and Smull 2003a). Many blocked-flow events feature near-barrier cold pools and/or cold-air damming (e.g., Dunn 1987, 1992; Bell and Bosart 1988; Colle and Mass 1995; Overland and Bond 1995), whereas there were no strong near-barrier contrasts in low-level θ and θ_{ei} near the barrier early in IOP3 and only a weak cold pool later. There were several reasons for this. First, events with near-barrier cold pools typically feature along-barrier cold advection (Braun et al. 1999). For example, along the eastern slopes of mountain ranges (e.g., the Rockies and Appalachians), blocked flow usually enhances the equatorward advection of cold air from the higher latitudes (e.g., Dunn 1987, 1992; Bell and Bosart 1988; Colle and Mass 1995). Paradoxically, in many cases of blocking along the western slopes of mountain ranges, there is a source of cold air from the lower latitudes, such as occurs when relatively cool marine air is advected poleward along the coastal ranges during a North American cold surge (e.g., Mass and Albright 1987; Mass and Steenburgh 2000). During IPEX IOP3, however, there was no source of cold air to the south (not shown) and the along-barrier flow was not associated with cold advection. Second, near-barrier cold pools during cold-air damming are frequently enhanced by upslope adiabatic cooling (e.g., Bell and Bosart 1988). For this to result in a near-barrier cold pool, however, the atmosphere must be stably stratified and during IPEX IOP3 the stratification was nearly moist-neutral. As a result, the saturated upslope ascent did not produce significant cooling relative to the environment. Finally, subcloud diabatic effects can create or enhance a near-barrier cold pool (e.g., Fritsch et al. 1992; Marwitz and Toth 1993). Such effects appeared to be responsible for the weak near-barrier cold pool that developed late in the event because of melting snowfall near the barrier. Upstream radiative surface heating further enhanced the weak low-level temperature contrast between the upstream sounding site and near-barrier cold pool.

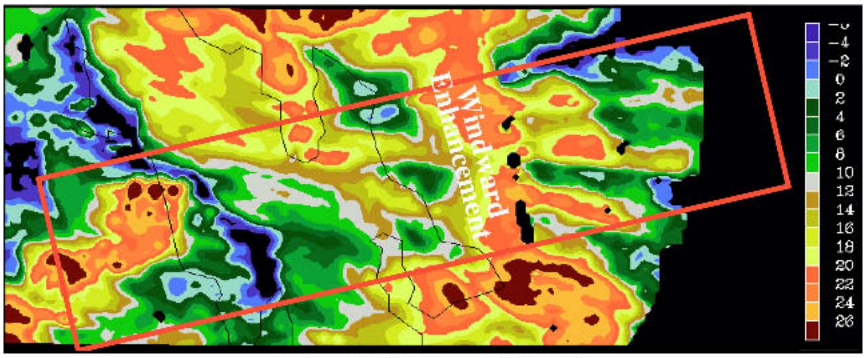

a) KMTX (2265 m, 2310 UTC)

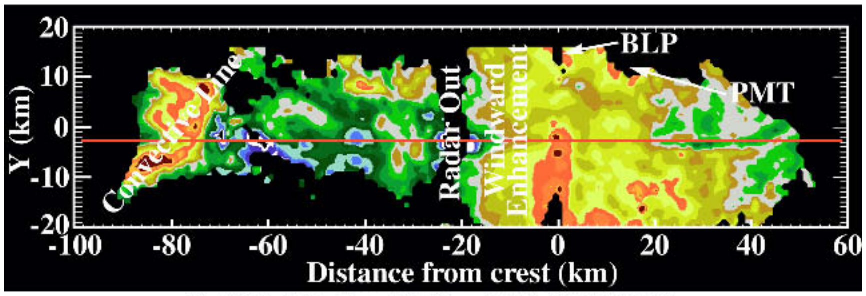

b) P3 Tail Radar (2640 m, 2312–2330 UTC)

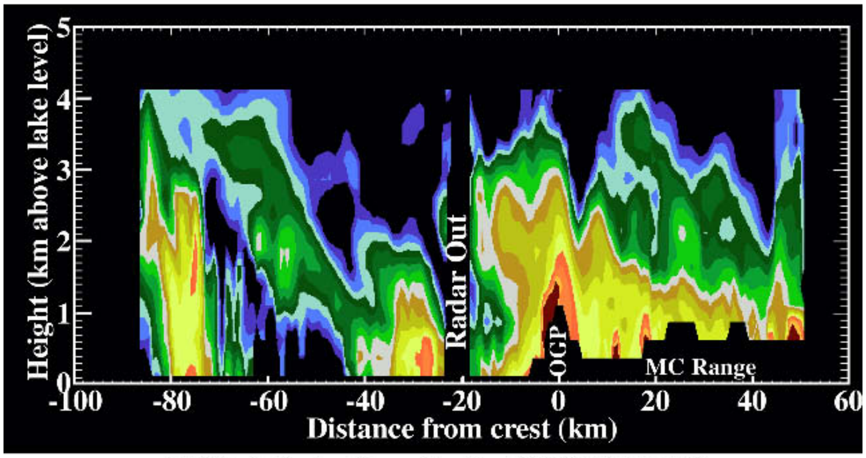

c) P3 Tail Radar Cross Section (2312–2330 UTC)

FIG. 16. Same as Fig. 4 except for (a) 2310 UTC 12 Feb 2000 and (b), (c) 2312–2330 UTC 12 Feb 2000.

There were also differences in the scale and depth of the along-barrier flow compared to prior studies. Elevation of the along-barrier jet core, due presumably to frictional slowing near the ground and observed in other blocked-flow events (Parish 1982; Bousquet and Smull 2003a), was not observed in this case. Instead, the jet-core was located at the lowest dual-Doppler level, suggesting that it was no more than 300 m above the surface compared with 1500–2000 m observed by Parish (1982) in the Sierra Nevada and Bousquet and Smull (2003a, see their Fig. 8c) in the Alps. The along-barrier flow also extended no more than 40 km upstream of the Wasatch Mountains, with the jet-core confined to within 5 km. Pierrehumbert and Wyman (1985) found that the decelerated flow zone should extend a Rossby radius, *Nh/f*, upstream of the barrier, before retreating toward the mountain. In this case, the 40-km maximum upstream extent of the decelerated flow zone was somewhat smaller than the calculated Rossby radii of 50–100 km. Pierrehumbert and Wyman (1985) did not consider, however, saturated flow under near-moist-neutral stratification, as was observed during IOP3. Rotunno and Ferretti (2001) appears to be the only comprehensive study of flow over an orographic barrier

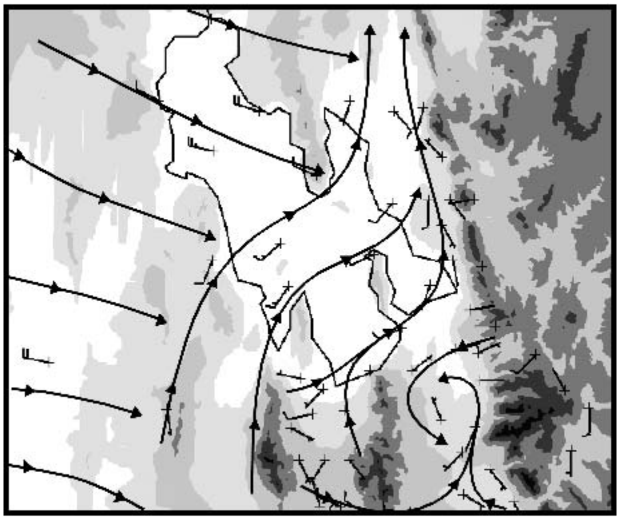

FIG. 17. Manual streamline analysis at 2300 UTC 12 Feb 2000.

under such conditions. Using idealized numerical simulations, they found that a horizontally uniform, saturated, moist-neutral flow is able to surmount an Alps-like barrier with little or no upstream flow deflection. A narrow zone of blocked flow could be produced, however, if they introduced a small gradient in saturation deficit (i.e., relative humidity) along the barrier, with the driest air to the right when looking downstream at the barrier. Since the low levels to the south (i.e., over the Salt Lake and Tooele Valleys) were weakly subsaturated for much of the event, it is possible that similar processes contributed to the structure of IOP3. On the other hand, IOP3 differed from the event examined by Rotunno and Ferretti (2001) in the structure of the large-scale flow [e.g., IOP3 featured reversed shear with height just above crest level, whereas the Rotunno and Ferretti (2001) idealized simulations used a barotropic wind profile] and the narrowness of the Wasatch Mountains compared to the Alps. These factors have been shown to have dramatic impacts on atmospheric flows across mountain barriers under dry, statically stable conditions (e.g., Durran 1986). Thus, additional research is needed to better understand the influence of the Wasatch Mountains on the flow patterns observed during IOP3.

The kinematic structure of IOP3 may also have been influenced by lake–land roughness contrasts and orographic effects associated with the topography found south of the Great Salt Lake. During IOP3, southwesterly flow was directed toward the eastern, meridionally oriented shore of the Great Salt Lake, a situation

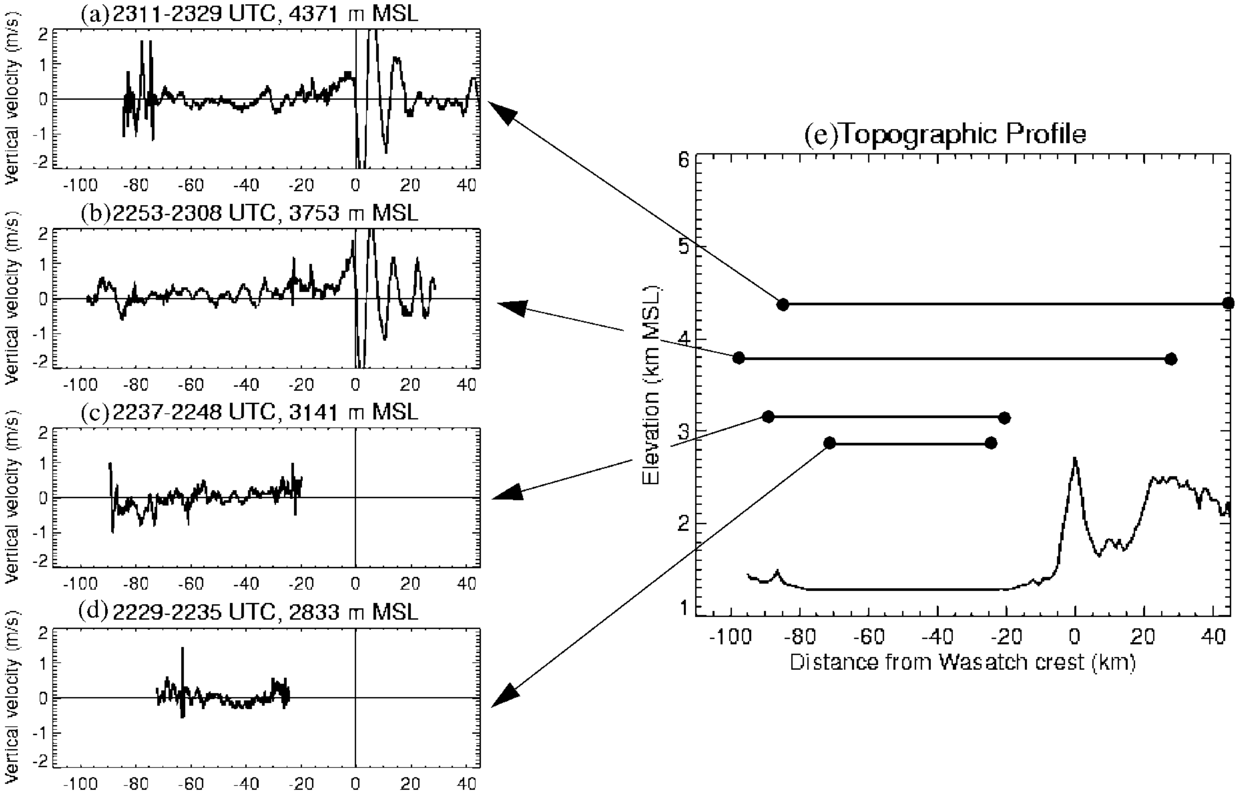

FIG. 18. WP-3D flight level vertical velocities (w) during stack 4 (2229–2329 UTC 12 Feb 2000) at (a) 4371, (b) 3753, (c) 3143, and (d) 2833 m MSL.

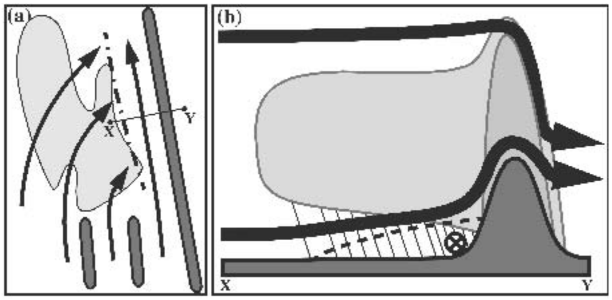

FIG. 19. Schematic diagram summarizing the kinematic and precipitation structure of IOP3. (a) Surface streamlines and convergence zone (dashed–dotted) with Great Salt Lake and major topographic features indicated by light and dark shading, respectively. (b) Cross section [along X–Y of (a)] illustrating windward precipitation region (light shading indicating snow, with hatching illustrating rain below the melting level), localized precipitation maximum centered on the crest (medium shading), along-barrier jet (circle with embedded X), transition region from along to cross-barrier flow (dashed line), and streamlines indicating intense near-barrier ascent and lee wave.

shown by Roeloffzen et al. (1986) to be favorable for flow deceleration and veering winds as the flow moves over the increased roughness of the land surface. In addition, the presence of the Oquirrh and Stansbury Mountains essentially results in southerly, along-barrier flow occurring farther upstream than if the flow incident on the Wasatch were unperturbed. Both factors may have contributed to the strength and positioning of the windward convergence zone during IPEX IOP3. Sensitivity studies using a numerical model are needed to determine the relative importance of these factors in modifying the windward convergence zone, when compared to other factors like static stability and slope steepness.

c. Submesoscale circulations and precipitation features

The radar analysis presented in this paper also revealed a number of submesoscale flow and precipitation features. Dual-Doppler winds revealed strong upcanyon flow in major mountain gaps like Ogden and Weber Canyons. Thus, the Wasatch Range is essentially a "leaky barrier" with the canyons providing a conduit for low-level air to move across the barrier. This upcanyon flow contrasts with the diabatically cooled downvalley flow that helped maintain the low-level cold pool observed during an Alpine precipitation event featuring blocking (Steiner et al. 2003; Bousquet and Smull 2003a), and is more consistent with the upvalley flow observed by Bousquet and Smull (2003b) during an unblocked Alpine precipitation event. There was also no evidence of precipitation-induced downdrafts near the windward slopes, such as those observed in other Wasatch storms by Hill (1978). Near crest level, flow deflection and splitting were observed upstream of most major peaks. This flow splitting did not appear to have a major impact on the precipitation structure of the event. Locally heavy precipitation was observed, however, over BLP, which extends about 10 km westward from the general orientation of the Wasatch Crest, was oriented more normal to the incident flow, and experienced stronger cross-barrier flow.

5. Summary and conclusions

This paper has described the kinematic structure of a winter storm over the Wasatch Mountains of northern Utah using observations collected during IOP3 of the Intermountain Precipitation Experiment (IPEX). IOP3 featured the passage of a midlevel (700–550 hPa) trough followed 3 h later by a trailing surface trough. Crest-level winds prior to and during midlevel trough passage were southwesterly to westerly and oriented roughly normal to the Wasatch Mountains where substantial orographic precipitation enhancement was observed. Although precipitation generally increased with elevation, precipitation enhancement occurred over the lowlands upstream of the initial Wasatch slope near Ogden, Utah. Kinematic and radar data provided by the NOAA WP-3D research aircraft and two Doppler on Wheels (DOW) radars showed that this precipitation enhancement was produced by low-level convergence between large-scale southwesterly flow and along-barrier flow near the Wasatch Mountains. A pronounced "reflectivity wall," characterized by vertically oriented isoechos, was collocated with the convergence zone and demarcated the windward precipitation region. The along-barrier flow, convergence zone, and reflectivity wall collapsed toward the barrier during and following the passage of the midlevel trough. Meanwhile, southwesterly and westerly flow with a substantial cross-barrier component produced a narrow region of strong ascent (1–2 m s^{-1}) near the windward slopes of the Wasatch Mountains at mid- to upper-mountain levels. This appeared to be responsible for the narrow reflectivity and precipitation maxima that were roughly centered on the Wasatch Crest. Mountain-wave-induced subsidence, which at times exceeded 2 m s^{-1}, was observed to the immediate lee of the barrier and, based on radar reflectivity analyses, appeared to limit hydrometeor spillover to the lee. The heaviest accumulations were observed on Ben Lomond Peak, where the local ridgeline was oriented normal to the upstream midmountain flow.

Although precipitation enhancement has been observed upstream of other mountain ranges (e.g., Peterson et al. 1991; Neiman et al. 2002; Medina and Houze 2003), IPEX IOP3 was unique in that it occurred under relatively weak stratification. The event also differed from many blocked-flow events since the near-barrier cold pool was weak and the horizontal scale of the along-barrier flow and the elevation of the embedded jet core were smaller than observed in previous studies. The lack of a strong near-barrier cold pool was the result of several factors. First, there was no along-barrier cold advection because of the absence of a cold-air source to the south. Second, because lapse rates were near moist neutral, saturated ascent did not generate a temperature deficit near the barrier. Finally, although the lack of substantial low-level dewpoint depressions limited the potential impact of evaporative cooling, diabatic cooling associated with melting snow, combined with upstream surface heating, did result in a weak cold pool late in the event.

Since very few studies have examined the upstream effects of mountains under saturated, moist-neutral conditions, theoretical work, combined with idealized and real-data numerical simulations, is needed to fully understand the mechanisms contributing to the development and evolution of the along-barrier flow and windward convergence zone. In addition to topographic blocking, increased surface drag at the east shore of the Great Salt Lake, as well as the presence of substantial topography upstream of the Wasatch to the south, may have also played a role. Nevertheless, the kinematic analysis presented in this paper, and future microphysical analyses of IOP3, should provide valuable datasets for verifying and improving numerical simulations of moist flow over a narrow, steeply sloped barrier, as well as quantitative precipitation forecasts in regions of complex terrain.

Acknowledgments. Funding for the analysis of data from IPEX was provided by National Science Foundation Grant ATM-0085318 and a series of grants provided by the National Weather Service C-STAR program to the NOAA Cooperative Institute for Regional Predication at the University of Utah. We would like to thank all the individuals and organizations who participated in the planning and execution of IPEX. Thanks also to the staff of the NOAA Aircraft Operations Center for their efforts in collecting airborne observations, the University of Oklahoma for providing the DOW units, the National Severe Storms Labs for operating the mobile labs, and Dick Oye of the National Center for Atmospheric Research for his assistance in the dual-Doppler analysis. Comments and suggestions provided by Larry Dunn, Mark Jackson, John Marwitz, David Schultz, and one anonymous reviewer greatly improved the manuscript.

REFERENCES

Atlas, D., R. C. Srivastava, and R. S. Sekhon, 1973: Doppler radar characteristics of precipitation at vertical incidence. *Rev. Geophys. Space Phys.,* **11,** 1–35.

Bell, G. D., and L. F. Bosart, 1988: Appalachian cold-air damming. *Mon. Wea. Rev.,* **116,** 137–161.

Blazek, T. R., 2000: Analysis of a Great Basin cyclone and attendant mesoscale features. M.S. thesis, Dept. of Meteorology, University of Utah, 122 pp. [Available from Department of Meteorology, University of Utah, 135 South 1460 East, Salt Lake City, UT 84112.]

Bougeault, P., and Coauthors, 2001: The MAP special observing period. *Bull. Amer. Meteor. Soc.,* **82,** 433–462.

Bousquet, O., and B. F. Smull, 2003a: Observations and impacts of upstream blocking during a widespread orographic precipitation event. *Quart. J. Roy. Meteor. Soc.,* **129,** 391–409.

——, and ——, 2003b: Airflow and precipitation fields within deep Alpine valleys observed by airborne Doppler radar. *J. Appl. Meteor.,* **42,** 1497–1513.

Braun, S. A., R. Rotunno, and J. B. Klemp, 1999: Effects of coastal orography on landfalling cold fronts. Part I: Dry, inviscid dynamics. *J. Atmos. Sci.,* **56,** 517–533.

Bruintjes, R., T. Clark, and W. Hall, 1994: Interaction between topographic airflow and cloud and precipitation development during the passage of a winter storm in Arizona. *J. Atmos. Sci.,* **51,** 48–67.

Bryan, G. H., and M. J. Fritsch, 2000: Moist absolute instability: The sixth static stability state. *Bull. Amer. Meteor. Soc.,* **81,** 1207–1230.

Colle, B. A., and C. F. Mass, 1995: The structure and evolution of cold surges east of the Rocky Mountains. *Mon. Wea. Rev.,* **123,** 2577–2610.

——, and ——, 1996: An observational and modeling study of the interaction of low-level southwesterly flow with the Olympic Mountains during COAST IOP4. *Mon. Wea. Rev.,* **124,** 2152–2175.

Cooper, W. A., and C. P. R. Saunders, 1980: Winter storms over the San Juan Mountains. Part II: Microphysical processes. *J. Appl. Meteor.,* **19,** 927–941.

Cox, J. A. W., 2002: Kinematic structure of a Wasatch Mountain snowstorm. M.S. thesis, Dept. of Meteorology, University of Utah, 60 pp. [Available from Department of Meteorology, University of Utah, 135 South 1460 East, Room 819, Salt Lake City, UT 84112-0110.]

Cressman, G. P., 1959: An operational objective analysis system. *Mon. Wea. Rev.,* **87,** 367–374.

Crum, T. D., R. L. Alberty, and D. W. Burgess, 1993: Recording, archiving, and using WSR-88D data. *Bull. Amer. Meteor. Soc.,* **74,** 645–653.

Dunn, L. B., 1987: Cold air damming by the Front Range of the Colorado Rockies and its relationship to locally heavy snows. *Wea. Forecasting,* **2,** 177–189.

——, 1992: Evidence of ascent in a sloped barrier jet and associated heavy-snow band. *Mon. Wea. Rev.,* **120,** 914–924.

Durran, D. R., 1986: Mountain waves. *Mesoscale Meteorology and Forecasting,* P. S. Ray, Ed., Amer. Meteor. Soc., 472–492.

——, and J. B. Klemp, 1982: On the effects of moisture on the Brunt–Väisälä frequency. *J. Atmos. Sci.,* **39,** 2152–2158.

Foote, G. B., and P. S. du Toit, 1969: Terminal velocity of raindrops aloft. *J. Appl. Meteor.,* **8,** 249–253.

Fritsch, J. M., J. Kapolka, and P. A. Hirschberg, 1992: The effects of subcloud-layer diabatic processes on cold air damming. *J. Atmos. Sci.,* **49,** 49–70.

——, and Coauthors, 1998: Quantitative precipitation forecasting: Report of the Eighth Prospectus Development Team, U. S. Weather Research Program. *Bull. Amer. Meteor. Soc.,* **79,** 285–299.

Fujita, T., 1963: Analytical mesometeorology: A review. *Severe Local Storms, Meteor. Monogr.,* No. 27, Amer. Meteor. Soc., 77–125.

Heggli, M. F., and R. M. Rauber, 1988: The characteristics and evolution of supercooled water in wintertime storms over the Sierra Nevada: A summary of microwave radiometric measurements taken during the Sierra Cooperative Pilot Project. *J. Appl. Meteor.,* **27,** 989–1015.

Hill, G. E., 1978: Observations of precipitation-forced circulations in winter orographic storms. *J. Atmos. Sci.,* **35,** 1463–1472.

Hobbs, P. V., 1975: The nature of winter clouds and precipitation in the Cascade Mountains and their modification by artificial seeding. Part I: Natural conditions. *J. Appl. Meteor.,* **14,** 783–804.

Horel, J., and Coauthors, 2002: Mesowest: Cooperative mesonets in the western United States. *Bull. Amer. Meteor. Soc.,* **83,** 211–225.

Huggins, A. W., 1995: Mobile microwave radiometer observations: Spatial characteristics of supercooled cloud liquid water and cloud seeding implications. *J. Appl. Meteor.,* **34,** 432–446.

Jorgensen, D. P., T. Matejka, and J. D. DuGranrut, 1996: Multibeam techniques for deriving wind fields from airborne Doppler radars. *J. Meteor. Atmos. Phys.,* **59,** 83–104.

Kain, J. S., S. M. Goss, and M. E. Baldwin, 2000: The melting effect as a factor in precipitation-type forecasting. *Wea. Forecasting,* **15,** 700–714.

Klimowski, B. A., and Coauthors, 1998: The 1995 Arizona Program: Toward a better understanding of winter storm precipitation development in mountainous terrain. *Bull. Amer. Meteor. Soc.,* **79,** 799–813.

Lazarus, S. M., C. M. Ciliberti, J. D. Horel, and K. A. Brewster, 2002: Near-real-time applications of a mesoscale analysis system to complex terrain. *Wea. Forecasting,* **17,** 971–1000.

Long, A. B., B. A. Campistron, and A. W. Huggins, 1990: Investigations of a winter mountain storm in Utah. Part I: Synoptic analyses, mesoscale kinematics, and water release rates. *J. Atmos. Sci.,* **47,** 1302–1322.

Marwitz, J. D., 1980: Winter storms over the San Juan Mountains. Part I: Dynamical processes. *J. Appl. Meteor.,* **19,** 913–926.

——, 1987a: Deep orographic storms over the Sierra Nevada. Part I: Thermodynamic and kinematic structure. *J. Atmos. Sci.,* **44,** 159–173.

——, 1987b: Deep orographic storms over the Sierra Nevada. Part II: The precipitation process. *J. Atmos. Sci.,* **44,** 174–185.

——, and J. Toth, 1993: The Front Range blizzard of 1990. Part I: Synoptic and mesoscale structure. *Mon. Wea. Rev.,* **121,** 402–415.

Mass, C. F., and M. D. Albright, 1987: Coastal southerlies and alongshore surges of the west coast of North America: Evidence of mesoscale topographically trapped response to synoptic forcing. *Mon. Wea. Rev.,* **115,** 1707–1738.

——, and W. J. Steenburgh, 2000: An observational and numerical study of an orographically trapped wind reversal along the west coast of the United States. *Mon. Wea. Rev.,* **128,** 2363–2397.

Medina, S., and R. A. Houze Jr., 2003: Air motions and precipitation growth in Alpine storms. *Quart. J. Roy. Meteor. Soc.,* **129,** 345–371.

Mohr, C. G., and L. J. Miller, 1983: CEDRIC—A software package for Cartesian space editing, synthesis, and display of radar fields under interactive control. Preprints, *21st Conf. on Radar Meteorology,* Edmonton, AB, Canada, Amer. Meteor. Soc., 559–574.

Neiman, P. J., and M. A. Shapiro, 1993: The life cycle of an extratropical marine cyclone. Part I: Frontal-cyclone evolution and thermodynamic air–sea interaction. *Mon. Wea. Rev.,* **121,** 2153–2176.

——, F. M. Ralph, A. B. White, D. E. Kingsmill, and P. O. G. Persson, 2002: The statistical relationship between upslope flow and rainfall in California's coastal mountains: Observations during CALJET. *Mon. Wea. Rev.,* **130,** 1468–1492.

Overland, J. E., and N. A. Bond, 1995: Observations and scale analysis of coastal wind jets. *Mon. Wea. Rev.,* **123,** 2934–2941.

Parish, T. R., 1982: Barrier winds along the Sierra Nevada Mountains. *J. Appl. Meteor.,* **21,** 925–930.

Peterson, T. C., L. O. Grant, W. R. Cotton, and D. C. Rogers, 1991: The effect of decoupled low-level flow on winter orographic clouds and precipitation in the Yampa River Valley. *J. Appl. Meteor.,* **30,** 368–386.

Pierrehumbert, R. T., and B. Wyman, 1985: Upstream effects of mesoscale mountains. *J. Atmos. Sci.,* **42,** 977–1003.

Rauber, R. M., 1992: Microphysical structure and evolution of a central Sierra Nevada orographic cloud system. *J. Appl. Meteor.,* **31,** 3–25.

——, and L. O. Grant, 1986: The characteristics and distribution of cloud water over the mountains of northern Colorado during wintertime storms. Part II: Spatial distribution and microphysical characteristics. *J. Climate Appl. Meteor.,* **25,** 489–504.

——, ——, D. Feng, and J. B. Snider, 1986: The characteristics and distribution of cloud water over the mountains of northern Colorado during wintertime storms. Part I: Temporal variations. *J. Climate Appl. Meteor.,* **25,** 468–488.

Reinking, R. F., J. B. Snider, and J. L. Coen, 2000: Influences of storm-embedded orographic gravity waves on cloud liquid water and precipitation. *J. Appl. Meteor.,* **39,** 733–759.

Roeloffzen, J. C., W. D. Van Den Berg, and J. Oerlemans, 1986: Frictional convergence at coastlines. *Tellus,* **38A,** 397–411.

Rotunno, R., and R. Ferretti, 2001: Mechanisms of intense Alpine rainfall. *J. Atmos. Sci.,* **58,** 1732–1749.

Sassen, K., 1984: Deep orographic cloud structure and composition derived from comprehensive remote sensing measurements. *J. Climate Appl. Meteor.,* **23,** 568–583.

——, R. M. Rauber, and J. B. Snider, 1986: Multiple remote sensor observations of supercooled liquid water in a winter storm at Beaver, Utah. *J. Climate Appl. Meteor.,* **25,** 825–834.

——, A. W. Huggins, A. B. Long, J. B. Snider, and R. J. Meitín, 1990: Investigations of a winter mountain storm in Utah. Part II: Mesoscale structure, supercooled liquid water development, and precipitation processes. *J. Atmos. Sci.,* **47,** 1323–1350.

Schultz, D. M., and Coauthors, 2002: Understanding Utah winter storms: The Intermountain Precipitation Experiment. *Bull. Amer. Meteor. Soc.,* **83,** 189–210.

Shafer, J. C., 2002: Synoptic and mesoscale structure of a Wasatch Mountain winter storm. M.S. thesis, Dept. of Meteorology, University of Utah, 70 pp. [Available from Department of Meteorology, University of Utah, 135 South 1460 East, Room 819, Salt Lake City, UT 84112-0110.]

Smith, R., and Coauthors, 1997: Local and remote effects of mountains on weather: Research needs and opportunities. *Bull. Amer. Meteor. Soc.,* **78,** 877–892.

Steenburgh, W. J., 2004: One hundred inches in one hundred hours: Evolution of a Wasatch Mountain winter storm cycle. *Wea. Forecasting,* **19,** 1018–1036.

Steiner, M., O. Bousquet, R. A. Houze Jr., B. F. Smull, and M. Mancini, 2003: Airflow within major Alpine river valleys under heavy rainfall. *Quart. J. Roy. Meteor. Soc.,* **129,** 411–432.

Wexler, R., R. J. Reed, and J. Honig, 1954: Atmospheric cooling by melting snow. *Bull. Amer. Meteor. Soc.,* **35,** 48–51.

Wurman, J., J. Straka, E. Rasmussen, M. Randall, and A. Zahrai, 1997: Design and deployment of a portable, pencil-beam, pulsed, 3-cm Doppler radar. *J. Atmos. Oceanic Technol.,* **14,** 1502–1512.